

UNIVERSITY OF WATERLOO
FACULTY OF SCIENCE
DEPARTMENT OF PHYSICS AND ASTRONOMY

Detecting Tau Neutrinos In The Pacific Ocean

University of Alberta
Department of Physics
Edmonton, AB

Author:
Akanksha Katil

Supervisor:
Prof. Juan Pablo Yáñez Garza

Academic term: 3A
January 11, 2021

Abstract

The Pacific Ocean Neutrino Explorer(P-ONE) is planned to be deployed in Cascadia Basin, located close to Vancouver Island, in 2024. This large-scale Cherenkov detector will join a worldwide network of neutrino telescopes and holds exciting possibilities of unraveling new physics. High energy tau neutrinos are one such exciting channel that P-ONE could access. They must have an astrophysical origin, and could be used to confirm the flux previously observed by IceCube, the cubic kilometer neutrino telescope in Antarctica. The report here is a first attempt at developing an algorithm that can successfully distinguish tau neutrinos(ν_τ) from the background.

The simulation chain for the purposes of this study is setup using IceCube software. About 1 ν_τ event is expected to be detected in P-ONE if the algorithm is capable of identifying all the ν_τ events. Every year, greater than 0.2 ν_τ events can be identified from the background with a probability greater than 0.5.

Contents

1	Introduction	1
1.1	The Ghost Particle	1
1.2	Neutrino Telescope In The Deep Pacific: P-ONE	1
1.3	Neutrino Detection Principle	3
1.3.1	Cherenkov Radiation and DOMs	3
1.3.2	Neutrino Signatures	3
1.3.3	ν_τ Signatures	5
1.4	Importance of detecting astrophysical ν_τ	5
2	Simulation Chain for P-ONE	7
2.1	Neutrino Generation and Propagation	7
2.1.1	The GCD File	7
2.1.2	Neutrino Generator	8
2.1.3	PROPOSAL	9
2.2	Photon Generation and Propagation	10
2.2.1	STRings For Absorption Length in Water	10
2.2.2	Simulating Flasher	10
2.2.3	Optical Properties	12
2.3	Generating Hits and Recopulses in mDOM	16
3	Analysis	19
3.1	Expected Number of ν_τ Per Year in P-ONE	19
3.2	The Method	20
3.3	The Algorithm	21
3.4	Signal from Background	22
3.5	Improving the Number of ν_τ events per year	26
4	Conclusion and Next Steps	28
A	Testing PROPOSAL	31
A.1	Lepton Number	31
A.2	Book keeping in I3File	31
A.3	Other Tests	32
B	Identifying the Center of Gravity of Hits	33
C	Bifurcated gaussian	35

D Suspicious ν_e Event	36
E Tau Decays into a muon	37
F More on Next Steps	38
G Documentation	40
G.1 Code	40
G.2 Weekly, Analysis and Collaboration meet presentations	40
G.3 Documenting Fits	40

Chapter 1

Introduction

1.1 The Ghost Particle

Often referred to as the ghost particles, neutrinos are the most abundant particles in the universe. Despite their abundance, the neutrino is the only particle in the standard model that does not interact strongly or electromagnetically, which means that it interacts very seldom [1]. First proposed by Wolfgang Pauli in 1930 [2], neutrinos have never failed to surprise physicists. Initially predicted to be massless in the standard model, the first neutrino oscillation evidence provided by SuperKamioka in 1998, showed that the neutrinos were indeed massive particles [2]. This in turn gave a palpable evidence of physics beyond the standard model.

1.2 Neutrino Telescope In The Deep Pacific: P-ONE

Given their small interaction cross-section [3], neutrinos open a new avenue to understand the cosmos at high energies, never explored before since the universe becomes opaque to photons in these high energies [4]. However, the caveat is that at high energies(50 TeV) the earth starts to become less transparent to neutrinos [4]. At 100 TeV only 20% of the neutrinos cross earth at zenith $\cos(\theta) = -0.8$ [4]. This calls for a network of neutrino telescopes to get an all sky exposure. Along with the current neutrino telescopes(ANTARES and IceCube) and the upcoming neutrino telescopes(KM3Net, Baikal-GVD and IceCube Gen-2) a near future P-ONE will cover the entire sky in search for high energy neutrinos(fig 1.1) [4].

The Pacific Ocean Neutrino Experiment(P-ONE) is a novel initiative to construct a multi-cubic telescope in Cascadia Basin(fig 1.2), several miles off shore to Vancouver Island in Canada [4]. Partnered with Ocean Networks Canada, P-ONE aims to expand the observable window to understand the universe at high energies. The P-ONE explorer planned to be deployed will not only provide insight for a complete installation of 70 string P-ONE but also start improving the existing search of high energy neutrinos [4].

The P-ONE explorer will consist of 10 Strings and 200 Digital Optical Modules(DOMs)(fig 1.3) [4]. The complete P-ONE will contain 6 more segments similar to the P-ONE explorer(fig 1.3) [4]. This segmented design was inspired from DUMAND [4]. The segmented

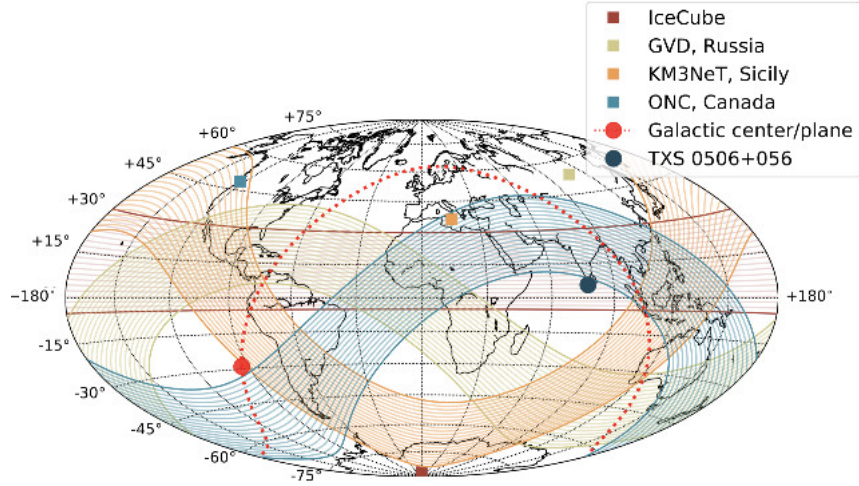


Figure 1.1: Neutrino telescopes, existing and under construction, around the globe with their horizontal coverage from which high energy neutrinos will not be affected by the Earth absorption. (Credit: M. Huber/TUM) Taken from [5]

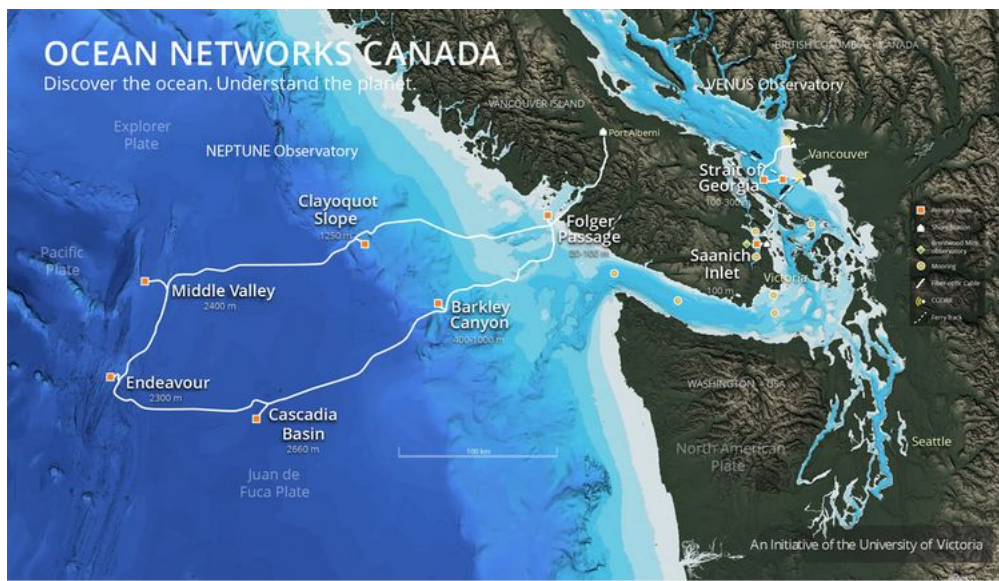


Figure 1.2: Map of ONC's NEPTUNE observatory: P-ONE will be installed at the node at Cascadia Basin at a depth of 2660 meter. (Credit: Ocean Network Canada). Taken from [6]

array would reduce the number of mooring lines without loosing out on the necessary information for reconstruction [4].

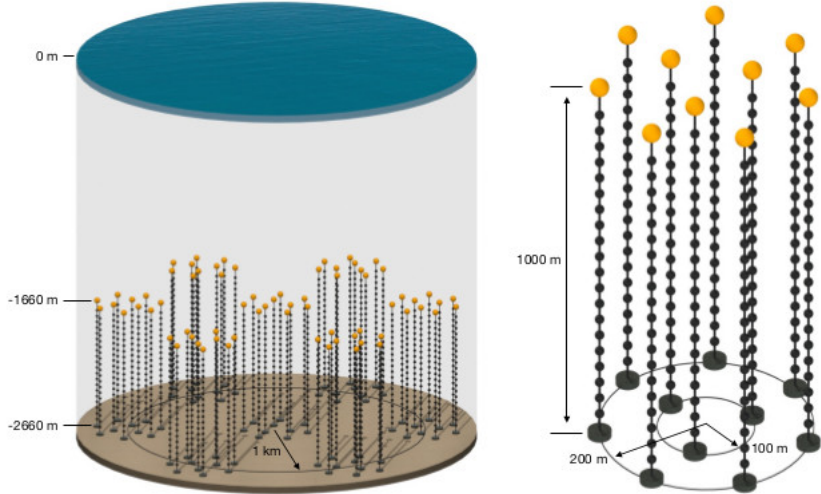


Figure 1.3: Design of the proposed final stage of instrumentation of the Pacific Ocean Neutrino Experiment consisting of seven segments optimized for energies above 50 TeV (left) and the design of an individual segment that is planned to be installed in a four weeks sea operation in 2023/24 as Pacific Ocean Neutrino Explorer standalone detector. (Credit: TUM). Taken from [7]

1.3 Neutrino Detection Principle

1.3.1 Cherenkov Radiation and DOMs

High energy neutrinos are detected using cherenkov radiation[8]. Analogous to the sonic boom, cherenkov radiation is emitted when a charged particle travels faster than the speed of light[9]. Cone of emission is the signature effect of cherenkov radiation[9].

The cherenkov radiation produced by neutrino interaction are detected by DOMs. A DOM houses either a single or multiple Photo-Multiplier Tube(PMT) and electronics. The photons emitted during the neutrino interaction hit the grounded photo-cathode, exciting the electrons[11]. These electrons are accelerated by the focusing electrode onto the first dynode[11]. The electrons are multiplied by secondary emission at the first dynode[11]. This process is repeated at other dynodes[11]. The electrons from the last dynode are collected at the high potential anode[11]. The digitizer then converts this to waveforms[8].

1.3.2 Neutrino Signatures

Each neutrino interaction can be categorized as a Charged Current(CC) interaction or a Neutral Current(NC) interaction[10]. When the neutrino produces a charged lepton through the exchange of a W-boson with a nucleon it is called a CC interaction[10]. But when the neutrino scatters by exchanging a Z-boson with a nucleon it is called a NC interaction(fig 1.6) [10]. In both CC an NC the energy transferred to the nucleon produces a secondary hadronic showers[10].

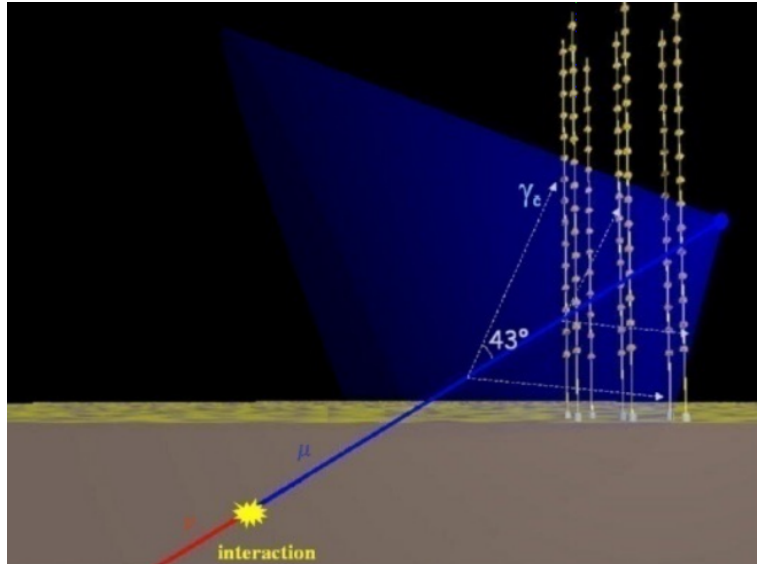


Figure 1.4: Schematics of neutrino detection in a water Cherenkov telescope: A neutrino(red line) interacts with a nucleus producing a muon (blue line). The muon induces the radiation of Cherenkov photons (blue cone) that can be detected by photo sensors(yellow dots). Credit: ANTARES Collaboration.Taken from [10]

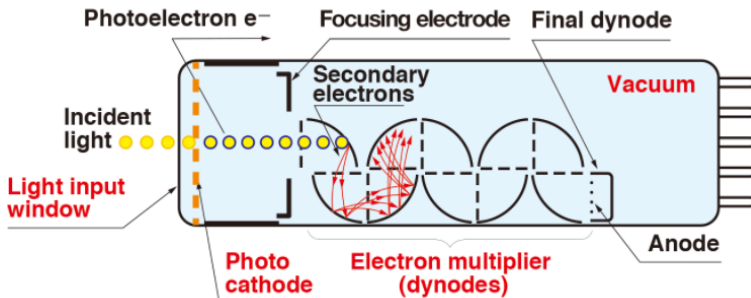


Figure 1.5: Construction of PMT. Taken from [12]

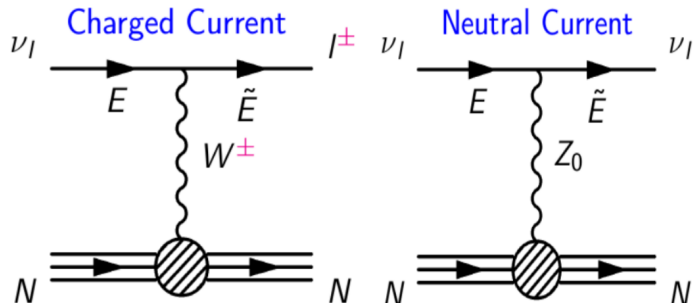


Figure 1.6: The Feynman diagrams for charged-current and neutral-current neutrino interactions with a nucleon. The difference between the two is the weak boson exchanged and the outgoing lepton. Taken from [3]

The three different flavours of neutrinos electron neutrino(ν_e), muon neutrino(ν_μ) and tau neutrino(ν_τ) can be differentiated using the topologies observed. Two basic topologies can be found in neutrino detectors[8]: 1)Tracks - produced by ν_μ 2)Cascades produced by ν_e , ν_τ and all flavoured NC interactions.

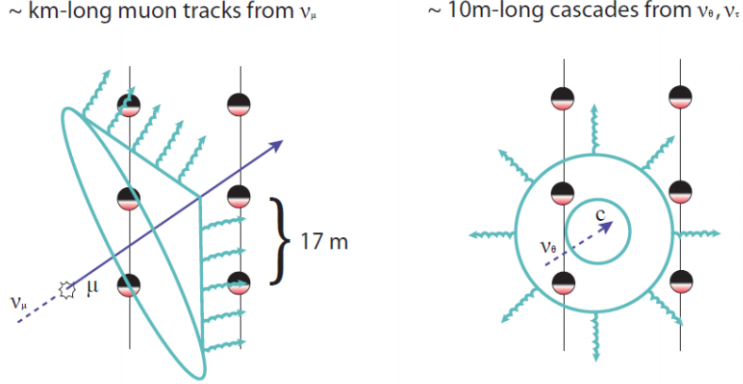


Figure 1.7: Contrasting Cherenkov light patterns produced by muons (left) and by showers initiated by electron and tau neutrinos (right) and by neutral current interactions. The patterns are often referred to as tracks and cascades (or showers). Cascades are produced by a (approximately) point source of light with respect to the dimensions of the detector. Taken from [8]

1.3.3 ν_τ Signatures

High energy ν_τ produce a very distinctive signature of double cascades, due to the fact that there are two vertices, the tau(τ) creation corresponds to the first vertex and τ decay corresponds to the second vertex[13]. The τ lifetime sets the distance between the two vertices[3]. There exists two different techniques to identify the double vertex namely double bang and double pulse signatures[13]. In a double bang signature the two vertices are observed in two different strings[13]. The double vertices should be separated by 100s of kilometers and the energy of the ν_τ is usually in some multi PeV range[13]. A double pulse signature is, however, observed in a single DOM in which two consecutive signals are produced[13]. The vertices are usually separated by 10s of kilometers with the ν_τ energy in 100s of TeV[13].

1.4 Importance of detecting astrophysical ν_τ

ν_τ are not usually produced in the atmosphere and they exist only due to neutrino oscillations[13]. Their observation in neutrino detectors will reaffirm the astrophysical origins of high energy neutrinos observed so far[14]. Despite the flavour ratio at a source produced by pion decays is $\nu_e : \nu_\mu : \nu_\tau = 1:2:0$, due to oscillations the observed ratio on earth is expected to be $\nu_e : \nu_\mu : \nu_\tau = 1:1:1$ [14]. Therefore ν_τ detection would also confirm the existing theories of neutrino oscillations on cosmological scales[13].

ν_τ are expected to contribute to 20% to 40% of the total astrophysical neutrino flux[13]. After 10 years of its construction, IceCube, the cubic kilometer detector in the south pole, is on the verge of detecting the first ν_τ with 90% C.L[13]. There are already three interesting ν_τ candidates discovered in IceCube[15]. Out of the three events one is a possible signal

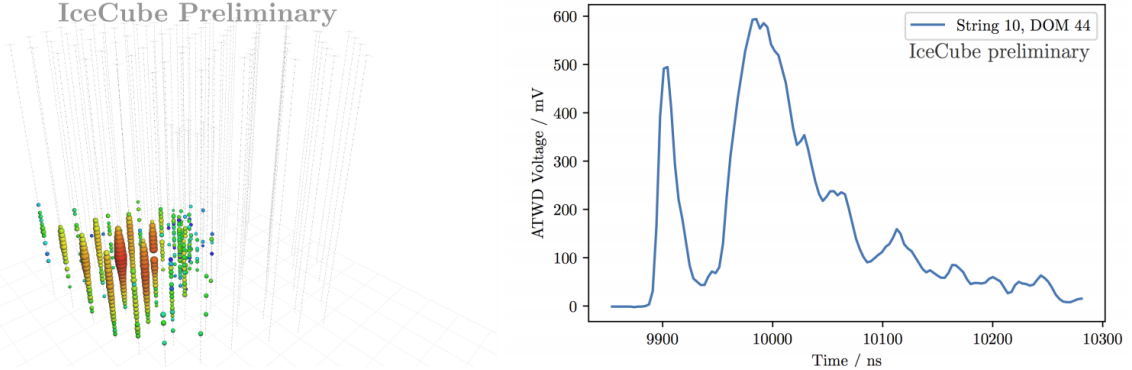


Figure 1.8: Left: Event view of the double pulse event recorded in the 2015 season in IceCube. Right: Double pulse waveform recorded for this event. Taken from [14]

event, one probable event and one certain background event[15]. The scattering in the ice makes it hard to see a double pulse signature in IceCube, this is the cause for the low significance in detecting ν_τ in IceCube.

Since non observation of ν_τ can have severe implications on existing physics of neutrino oscillations and validity of high energy astrophysical neutrinos detected so far, detection of ν_τ is important and should be regarded as priority by future detectors[13].

In this report, the possibility of detecting ν_τ using the P-ONE geometry is explored. The detailed steps of simulation are laid out in chapter 2 along with the brief description of the IceCube software used for the simulations. The algorithm developed to distinguish between the ν_τ and the background is described in chapter 3 along with the results from the analysis.

Chapter 2

Simulation Chain for P-ONE

This analysis uses the IceCube software for simulation. The software consists of IceTray framework, the data storage classes, event viewer and input/output file utilities[16]. IceTray has modules written in C++, the modules can be accessed using a Python interface through Boost C++ Libraries[17]. Information about the simulated events are stored in frames. These frames are usually preceded by files known as GCD which contain the Geometry, Calibration and Detector status information.

Various modules are used to produce a complete simulation chain. Some of the modules were already included in the IceCube software whereas others were developed solely for the purpose of P-ONE. The flow chart below (fig 1.2) gives a simple gist of the simulation chain.

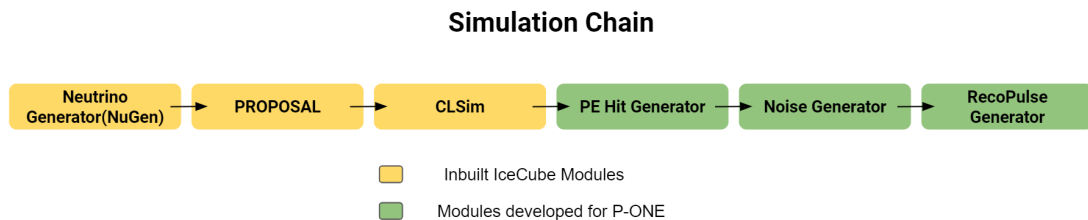


Figure 2.1: Simulation chain for ν_τ analysis

2.1 Neutrino Generation and Propagation

2.1.1 The GCD File

Before the neutrinos could be simulated, a new GCD file is generated for P-ONE. The geometry of the detector is modified to match that of the P-ONE phase 1 geometry(fig 2.2). The calibration and detector status were built using information taken from a single DOM from the IceCube GCD file. The calibration and detector status, containing information about IceCube DOM and PMT responses, are irrelevant to the analysis conducted here but crucial for the simulation to work properly.

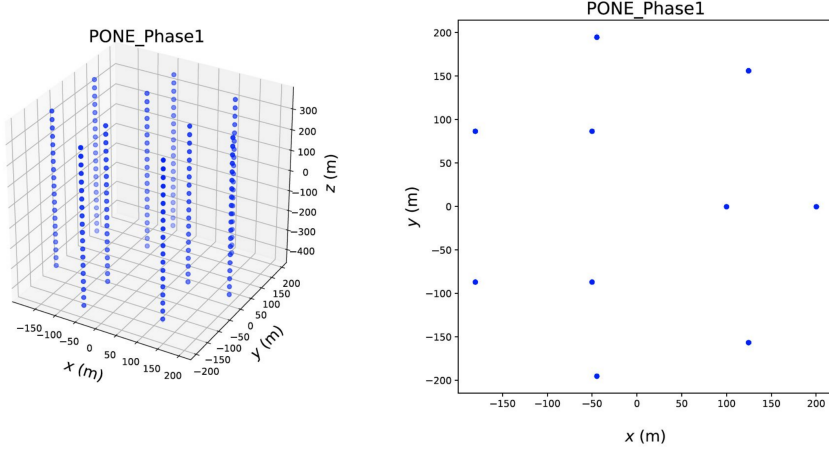


Figure 2.2: P-ONE geometry in python

2.1.2 Neutrino Generator

Neutrino Generator(NuGen) generates neutrinos and anti-neutrino based on the input flavours and flavour ratios. Both ν_τ and ν_e were simulated along with their corresponding anti particles. The flavour ratio was chosen to be $\nu_\tau : \bar{\nu}_\tau : \nu_e : \bar{\nu}_e = 1 : 1 : 1 : 1$. The energies of the neutrinos are sampled from a range of 100TeV - 5PeV according to the unbroken power law, in this case the power law was chosen to be $E^{-2.19}$ (fig 2.3). The value of the power law index was chosen according to flux model chosen for this analysis [18]. The azimuth and cos of zenith values of the neutrino were picked at random from the range 0-180 degrees.

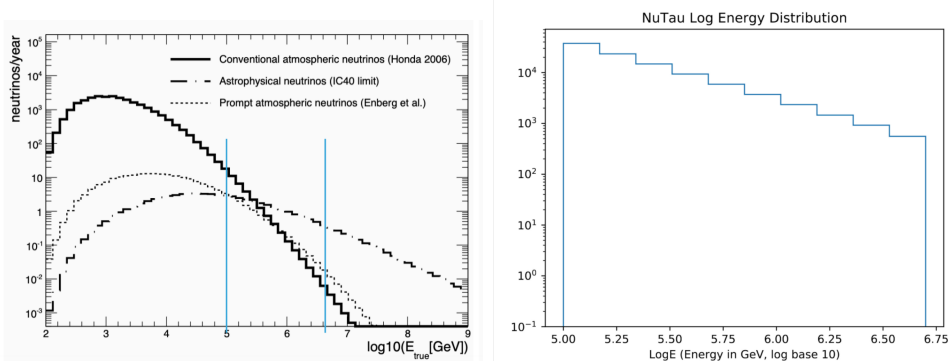


Figure 2.3: Left: Energy distribution of neutrinos. The Blue lines indicate the range from which the energies were sampled in the simulation. Right: Energy distribution of simulated neutrinos

The neutrinos are forced to interact by NuGen in the final simulation volume determined by the interaction cylinder. The size of the cylinder should be chosen appropriately since the detector is sensitive to interactions happening outside volume of the detector. The height and radius of the interaction cylinder are 1000 and 500 respectively(fig 2.4). The cylinder rotates so that it is always parallel to the z-axis of the neutrino simulated(fig 2.5) and thus eliminates the biases in certain angular directions. The true probability of the interaction is stored in I3MCWeightDict.

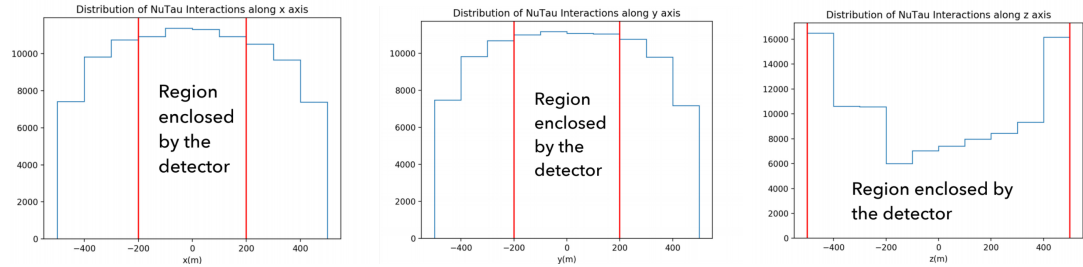


Figure 2.4: Interaction vertices of neutrino interaction are plotted. The regions enclosed by the detector are marked.

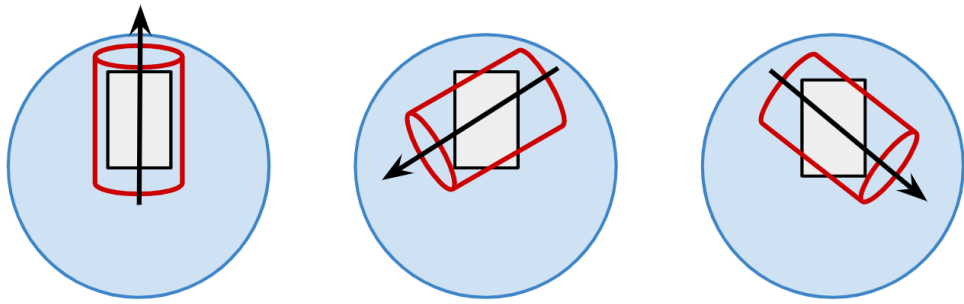


Figure 2.5: NuGen interaction cylinder. The arrow indicates the z-axis of the neutrino

2.1.3 PROPOSAL

IceCube module PROPOSAL was used to propagate the secondary charged particles produced from neutrino interaction in ice. The medium of propagation was not changed to water since the difference is negligible. To verify if τ are propagated as expected, the histogram of decay times of propagated taus in PROPOSAL is fit to an exponential curve defined by equation 2.1 (fig 2.6). The decay time from the fit is compared against the decay time calculated using the average energy of τ (Eq 2.2).

$$N = N_0 e^{-\frac{t}{T}} \quad (2.1)$$

where:

N_0 = Number of taus produced initially

T = Life time of tau in rest frame

$$T = \frac{E}{m} \tau \quad (2.2)$$

where:

E = Energy of tau

m = Mass of tau [1776.86 MeV]

τ = Lifetime of tau [2.9×10^{-4} ns]

For more tests done to examine the working of PROPOSAL see [Appendix A](#).

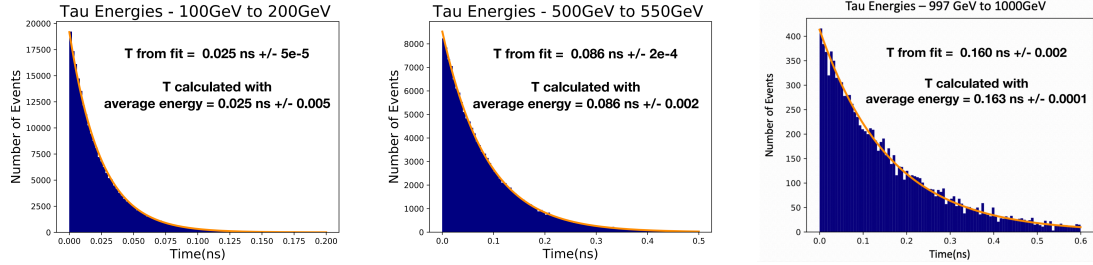


Figure 2.6: The Histogram of the τ decay times from the simulations is fit with curve defined by Eq 2.1. Decay time from both the fit and average energy are showed on the plots for comparison.

2.2 Photon Generation and Propagation

The next step is simulating the light yield from the propagated particles(stored as I3Particles in the frame) and then propagating these photons in the medium. The generation and propagation of the photons is done using the CLSim. The output of CLSim constitutes photons(stored as I3Photons) that enter the DOM region without being absorbed by the medium. CLSim uses GPUs for simulations. The simulation can be made computationally less intensive by turning off Geant4 option. Once Geant4 is turned off CLSim uses parameterized light emission instead of tracking individual particles.

A medium model should be given to CLSim. The medium should be simulated as close as possible to that of the Cascadia Basin for the best results. Therefore, the scattering and absorption lengths determined from STRings For Absorption Length in Water(STRAW) data are used to find the necessary parameters to be fed to the simulation scripts.

2.2.1 STRings For Absorption Length in Water

The optical properties of the Cascadia Basin are being studied using STRAW. The STRAW setup as shown in fig 2.7 consists of two mooring lines. The 435 kg buoy helps keep the mooring lines upright [19]. The STRAW array consists of 3 light emitting modules called the Precision Optical Calibration Module(POCAM) and 5 light sensing modules called STRAW Digital Optical Module(sDOM) [19]. Each sDOM houses two 3" PMTs, one facing upwards and one facing downwards [19]. The light flashes from the POCAM are recorded by the sDOM [19].

The integrating sphere around the POCAM ensures an almost isotropic light emission. The full width half maximum (FWHM) of the LED flasher is less than 10 ns. The LEDs are carefully selected to cover the wavelength range of 350 nm to 600 nm which is usually the wavelength of Cherenkov light.

2.2.2 Simulating Flasher

To test the optical medium, flashers are simulated in CLSim. The flasher should be identical to POCAM. Therefore, the flasher should emit isotropically in the selected wavelength with the Full Width Half Maximum(FWHM) similar to the LEDs POCAM houses. A script to simulate flashers already exists in IceCube software. Howbeit, this flasher is not isotropic in cosine of zenith(fig 2.8). Instead multiple flashers in cosine of zenith were

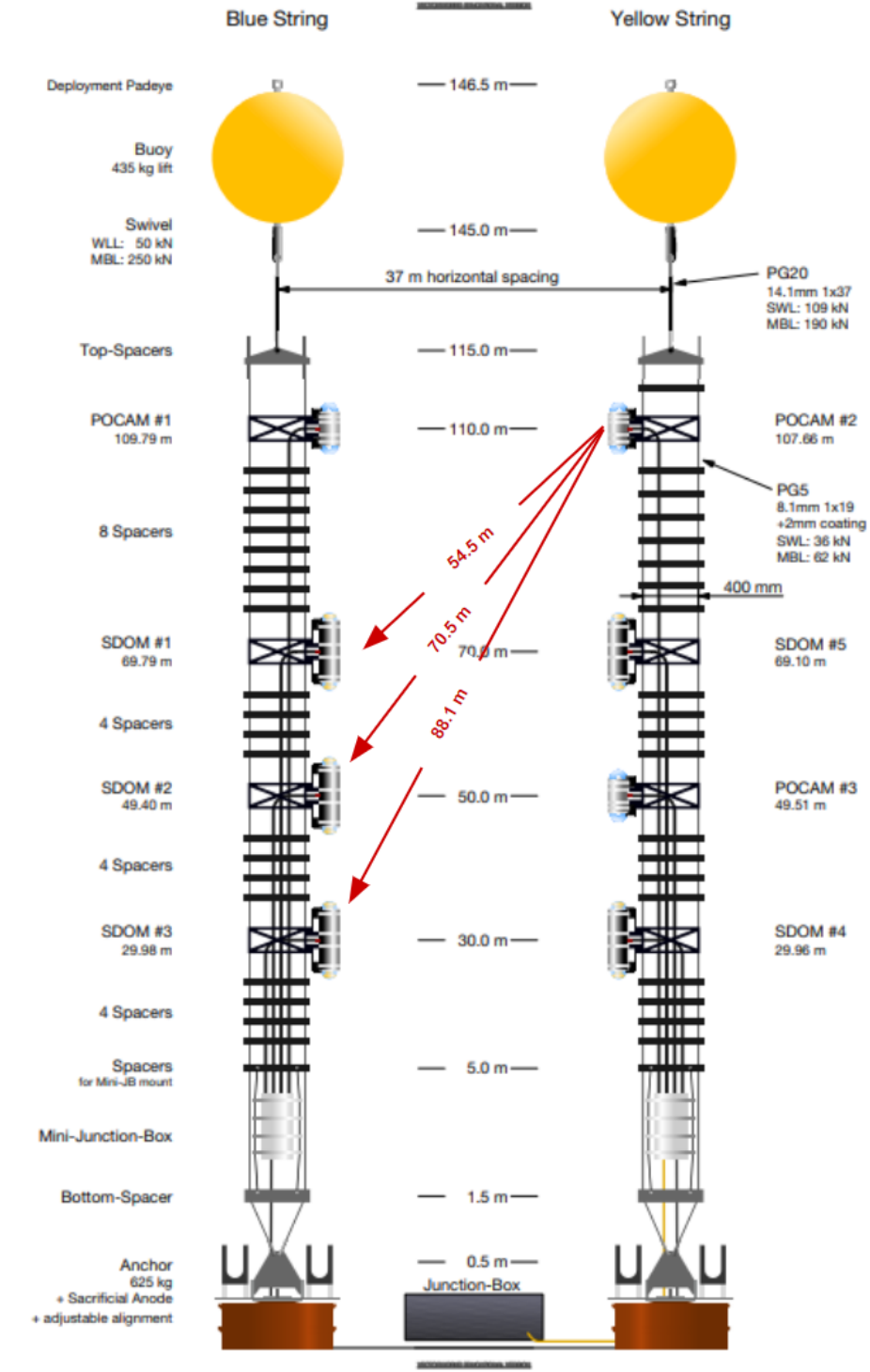


Figure 2.7: A detailed sketch of STRAW. Taken from [19]

simulated to get an isotropic emission in both cosine of zenith and azimuthal direction (fig 2.9). The FWHM of the pulse of multiple flashers is 10 ns (fig 2.10b). The number of flashers injected along cosine of zenith should be large. If a small number of flashers are injected, there are gaps observed near $\cos(0^\circ)$ and $\cos(180^\circ)$ (fig 2.10c).

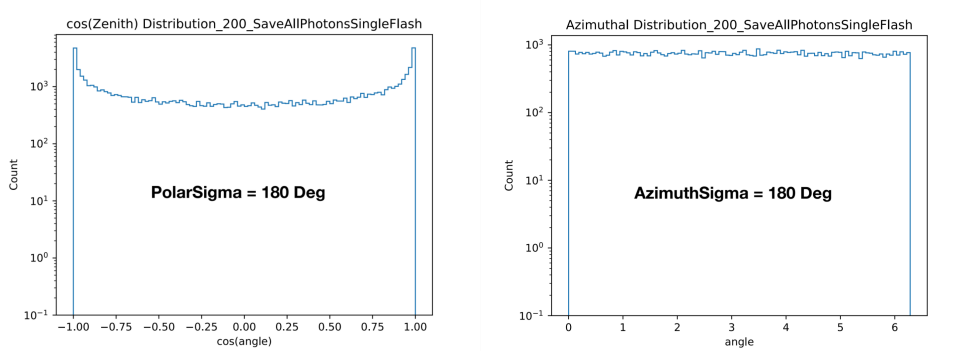


Figure 2.8: Left: The cosine of zenith distribution of the photons emitted from the flasher. Right: Azimuth distribution of the photons emitted by the flasher

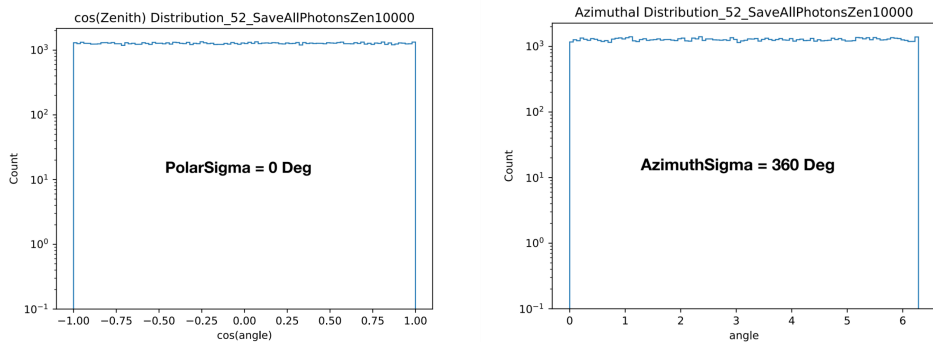


Figure 2.9: Left: The cosine of zenith distribution of the photons emitted from **multiple** flashers. Right: Azimuth distribution of the photons emitted from **multiple** flashers

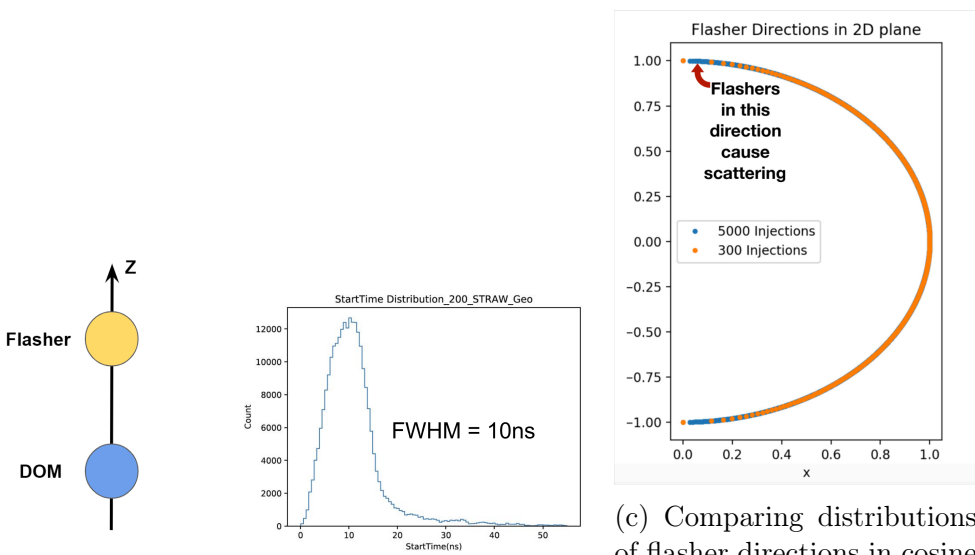
A set up as shown in fig 2.10a was used to replicate STRAW POCAM and sDOM. The distance between DOM and Flasher was varied according to the distances marked in fig 2.7.

2.2.3 Optical Properties

Majority of the work put in the direction of changing the optical medium to water in CLSim was done by Dvir Hilu, a previous co-op student.

The effective scattering coefficient $b_{e,400}$ and absorption coefficient $a_{dust,400}$ for 400 nm light measurements are tabulated with depth and temperature difference to reference depth of 1800m. For various wavelengths the medium is defined by the following equations [20]:

$$b_e = b_{e,400} \left(\frac{\lambda}{400} \right)^{-\alpha} \quad (2.3)$$



(a) The flasher setup used in the simulation. (b) The pulse shape of multiple flashers. The FWHM is same as that of POCAM. (c) Comparing distributions of flasher directions in zenith. More flashers cause scattering closer to $\cos(0)$ and $\cos(180^\circ)$

$$a = a_{dust,400} \left(\frac{\lambda}{400} \right)^{-\kappa} + Ae^{-B/\lambda}(1 + 0.01\Delta T) \quad (2.4)$$

The photon scattering angle θ (Eq 2.5) is modelled by using a linear combinations of Henyey-Greenstein(HG)(Eq 2.6) and Simplified Liu(SL)(Eq 2.7) [20].

$$p(\cos\theta) = (1 - f_{sl})HG(\cos\theta) + (f_{sl})SL(\cos\theta) \quad (2.5)$$

$$HG(\cos\theta) = \frac{1}{2} \frac{1 - g^2}{(1 + g^2 - 2g\cos\theta)^{\frac{3}{2}}} \quad (2.6)$$

$$SL(\cos\theta) = \frac{1 + \zeta}{2} \left(\frac{1 + \cos\theta}{2} \right)^\alpha, \zeta = \frac{2g}{1 - g} \quad (2.7)$$

where:

$$g = \langle \cos\theta \rangle$$

The ice model was specifically modeled for propagating photons in ice. Absorption and scattering coefficients change in ice with depth for every 10m but in water this is constant [20]. Using a least squares fit and the scattering and absorption lengths (fig 2.11) extracted, by Andreas Gaertner, from STRAW data, parameters in the above equations are determined. A and B values are manually set to zero since the exponential term in equation 2.4 is ignored due to the unavailability of scattering and absorption lengths at more wavelengths.

Using the simulated optical medium and flasher setup the time residuals (eq 2.8) are plotted. However, the shape of time residuals don't vary with increasing distance between

Wavelength(nm)	Scattering Length(m)	Effective Scattering Length(m)	Absorption Length(m)
365	32.30	163.16	9.21
405	56.78	286.81	17.56
465	66.87	337.78	31.87

Figure 2.11: Tabulating Scattering and Absorption length values for different wavelengths. A complete analysis is still in progress.

flasher and DOM (fig 2.12). This is because the $\langle \cos \theta \rangle$ value from Andreas Gaertner's study is zero. The $\langle \cos \theta \rangle$ is given as shown in equation 2.9 [21].

$$\text{Time Residual} = \text{Time the photon reaches DOM} - \text{Time the photon reaches DOM, if unscattered}$$

(2.8)

$$\langle \cos \theta \rangle = \eta \cdot \langle \cos \theta \rangle_{\text{molecular}} + (1 - \eta) \cdot \langle \cos \theta \rangle_{\text{particulate}}$$

(2.9)

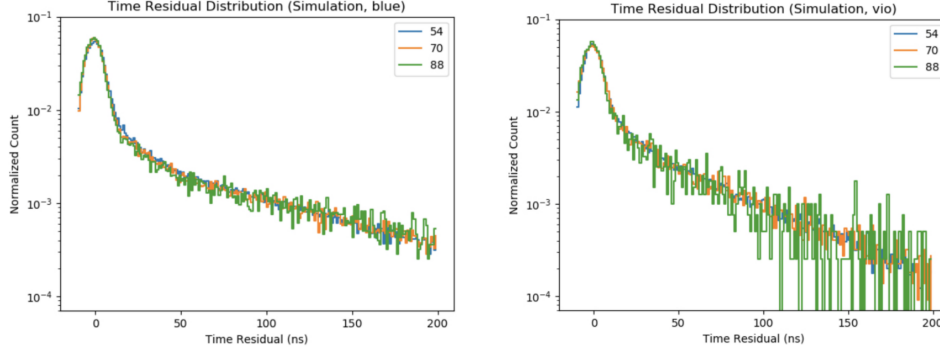


Figure 2.12: Time Residuals at different distances of simulation for blue and violet wavelengths

$\langle \cos \theta \rangle_{\text{particulate}}$ value is taken from ANTARES [21] and the ratio of molecular scattering η value is taken from Matthew Man's(a previous co-op student) analysis. And since the molecular phase function is symmetric around $\cos \theta = 0$, $\langle \cos \theta \rangle_{\text{molecular}}$ is zero. With $\langle \cos \theta \rangle$ not equal to zero anymore, scattering and effective scattering do not mean the same thing anymore. The effective scattering is given as[21]:

$$\lambda_{\text{sct}}^{\text{eff}} = \frac{\lambda_{\text{sct}}}{-\ln \langle \cos \theta \rangle}$$

(2.10)

Using equation 2.10 the effective scattering values for different wavelengths are computed (fig 2.11). The new effective scattering coefficient and the parameters in table 2.2.3 are inputted into the simulation. f_{sl} value is assumed to be zero since HG phase function is closer to the phase function used for STRAW analysis. Having changed the optical properties, time residuals are again plotted against the time residuals from STRAW data (fig 2.13). The time residuals from STRAW are saved as a histogram with 1 ns bin width usually. In certain instances the bin width was set to a smaller value. Now, the shape of the time residuals changes with distance (fig 2.14).

Parameters	Values
α	2.9
κ	5.08
$b_{e,400}$	0.0043
$a_{dust,400}$	0.065
A	0
B	0
η	0.132
$\langle \cos \theta \rangle_{\text{molecular}}$	0
$\langle \cos \theta \rangle_{\text{particular}}$	0.924
g	0.8
f_{sL}	0

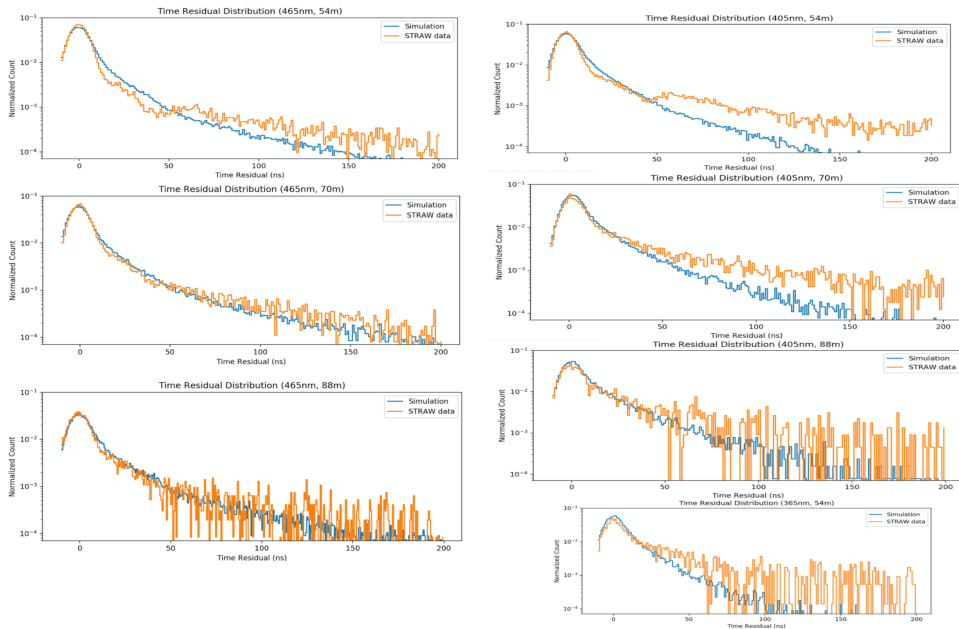


Figure 2.13: Time residuals simulation vs data

The time residuals from the simulation don't exactly match the data from STRAW near the tails. However, for this study the disagreement near the tail is not much of an issue.

Having set up the appropriate optical medium, CLSim was used to generate and propagate photons produced from the secondary particles generated from neutrino interactions in the medium. The photon weight accompanying every photon is dependent on the wavelength

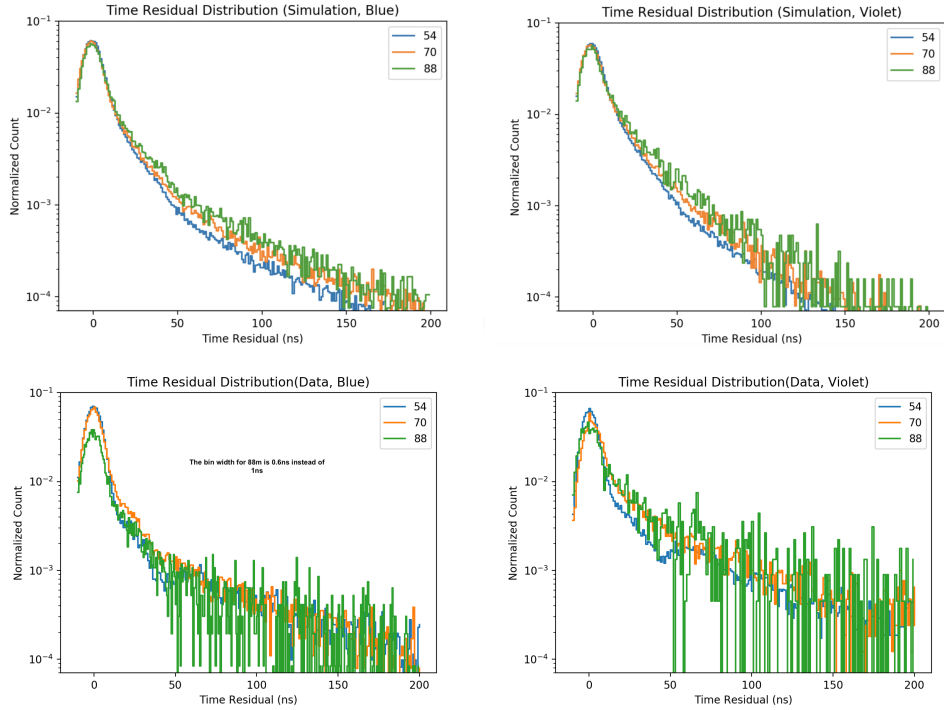


Figure 2.14: **Top:** Time Residuals at different distances from simulation for blue and violet wavelengths. **Bottom:** Time Residuals at different distances from data for blue and violet wavelengths

as seen in (fig 2.15), the wavelength distribution peaks at higher nanometeres when the photon weight is applied.

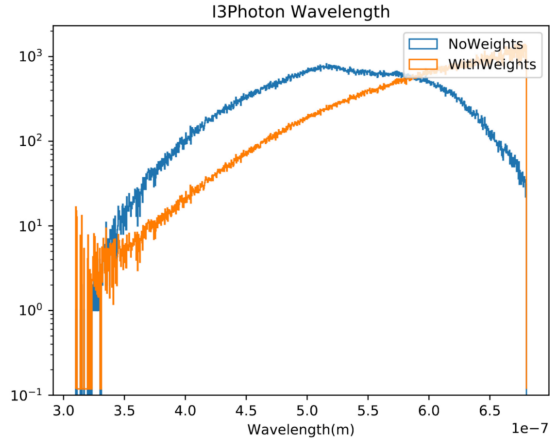


Figure 2.15: I3Photon wavelength distributions.

The next step in the simulation is generating hits.

2.3 Generating Hits and Recopulses in mDOM

Once the photon reaches the DOM region a probability of the photon making a hit is calculated using eq 2.11. If the probability is greater than the random number sampled from 0 - 1, the photon makes a hit. In this study an IceCube mDOM is simulated. The

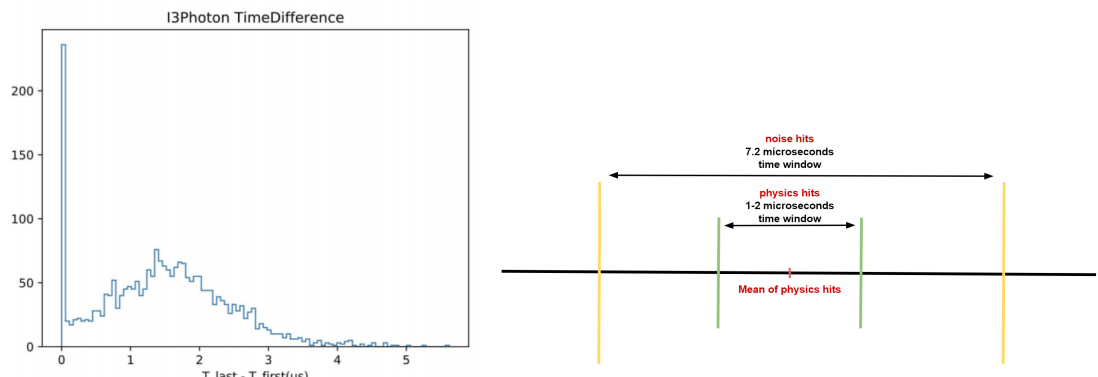
advantage of using an mDOM is that its angular acceptance is a constant [22]. The mDOM with 24 3" PMTs has 2.4 times more coverage area than an IceCube DOM [22], since area of 10" PMT is approximately equal to the area of ten 3" PMTs. The average of IceCube DOM acceptance is multiplied by a factor of 2.4, as the angular acceptance scales with the area. All the hits in an mDOM are aggregated and there is no information on which PMT the hit was generated in.

$$\text{Hit Probability} = \text{Relative DOM Eff} \times \text{DOM Eff} \times \text{Ang Acceptance} \times \text{Photon Weight} \quad (2.11)$$



Figure 2.16: mDOM Demonstrator Module. Taken from [22]

Data from the dark runs, runs where the POCAM is not flashing, from STRAW is injected in the simulation as noise. To inject noise on top of the physics hits a 7.2 microseconds time window is defined, this is the time that it takes a photon to traverse across P-ONE. Usually the time difference between the first photon that reaches a DOM and the last photon that reaches a DOM is between 0-3 microseconds(fig 2.17a). As there are 24 PMTs in a mDOM 24 random 7.2ns chunks of the STRAW data are selected and injected on top of physics hits in a single mDOM. The noise hits are injected so that they are centered around the mean of physics hits(fig 2.17b). The aggregate of noise and physics hits in each DOMs shown in figure 2.18.



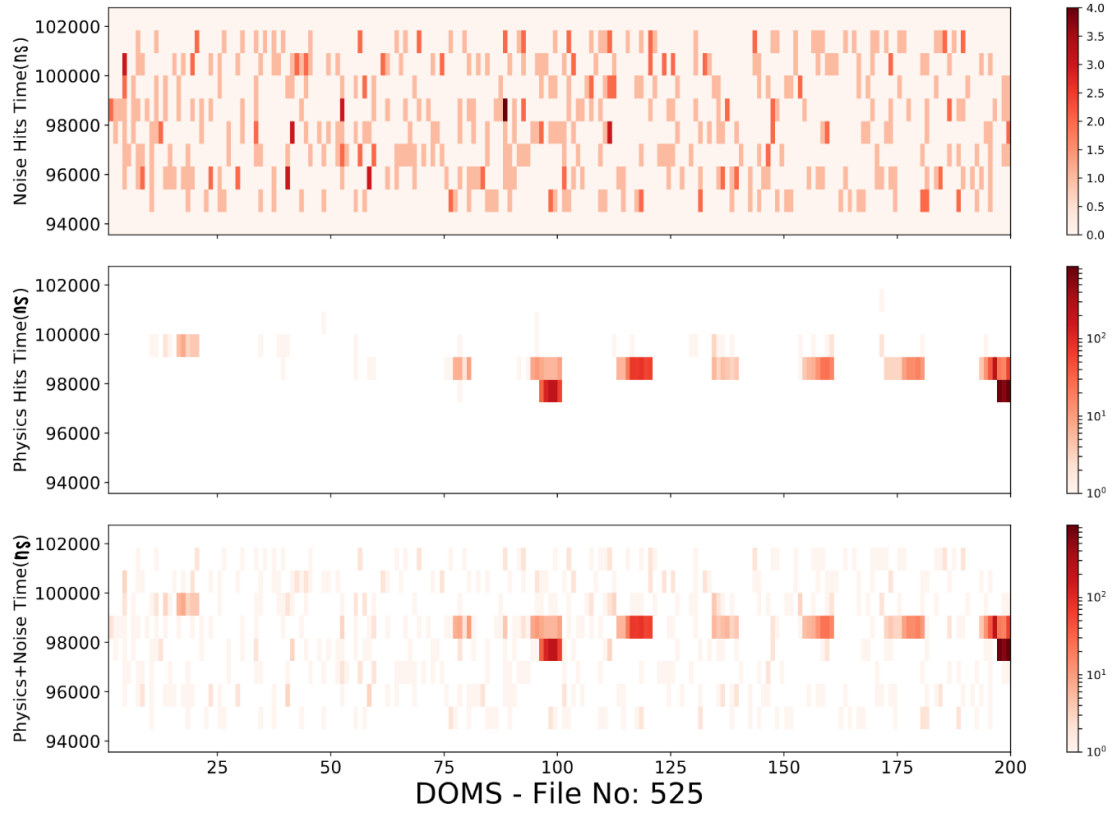


Figure 2.18: Noise + Physics hits in a single DOM. x axis: DOMs in P-ONE

Fake recopulses are generated and stored as I3RecoPulses. Hits within 3ns are merged as a single hit. The width of these recopulses is set as a constant and in this case the constant value is chosen as 3ns.

Chapter 3

Analysis

The analysis focuses on developing the algorithm that is capable of detecting the double pulse signature of ν_τ from the background. The main background in this study comes from:

1. CC interactions of ν_e
2. NC interactions of all flavoured ν
3. NC interactions of atmospheric ν_μ

3.1 Expected Number of ν_τ Per Year in P-ONE

To get the rough estimate of the number of ν_τ per year in P-ONE the events simulated need to be weighted first. Neutrino events simulated by using NuGen already come with an associated weight called OneWeight. Generation volume, interaction weight, propagation weight and spectral index are included in OneWeight. Using OneWeight the the events in the simulation are weighted(Eq 3.1) to match the desired flux(Eq 3.2)) [18].

$$weight = \frac{\phi_{astro} \times OneWeight}{N} \times LiveTime \quad (3.1)$$

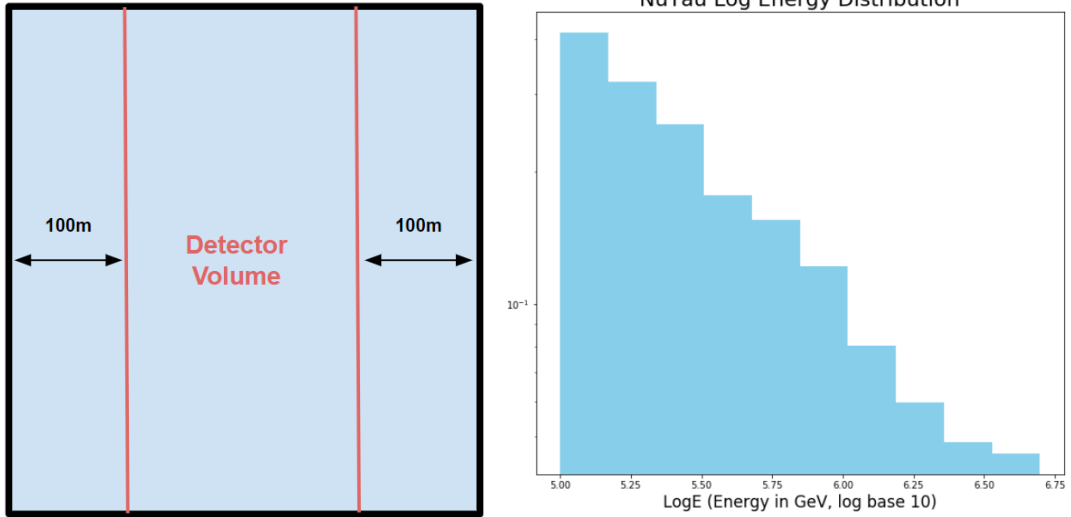
where:

N = Number of Tau neutrino events simulated

$LiveTime$ = Time the detector is turned on, in seconds

$$\frac{d\Phi_{\nu+\bar{\nu}}}{dE} = (1.01 \pm 0.26) \left(\frac{E}{100\text{TeV}} \right)^{-2.19 \pm 0.10} \cdot 10^{-18} \text{GeV}^{-1} \text{cm}^{-2} \text{s}^{-1} \text{sr}^{-1} \quad (3.2)$$

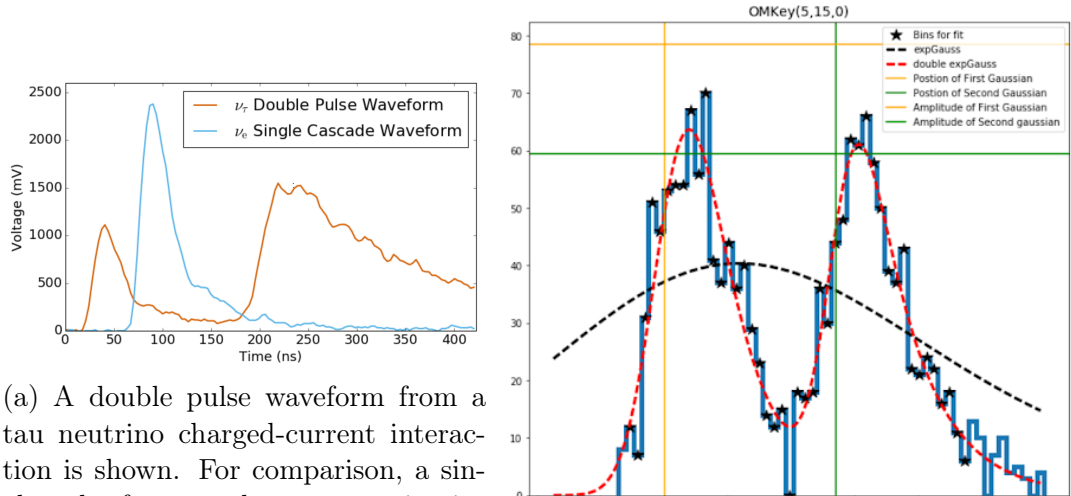
Only ν_τ CC interactions within a cylinder of height 1000m and radius 300m(fig 3.1a) are the desired events in this study. Events that satisfy this criteria are selected and their corresponding energies are histogrammed(fig 3.1b) according to the weights calculated. The resulting sum of total number of events in the bins, 1.68, is the number of events of CC ν_τ events per year in the selected volume.



(a) Volume considered for calculating the weight (b) Weighted energy distributions of CC ν_τ events within the volume shown in fig 3.1a

3.2 The Method

From fig 3.2a it is evident that ν_τ produces two gaussian like waveforms, whereas ν_e and NC interactions only produces a single gaussian like waveform. Fitting both a single and a double gaussian like functions to the data will show a separation between signal and background(fig 3.2b).



(a) A double pulse waveform from a tau neutrino charged-current interaction is shown. For comparison, a single pulse from an electron neutrino interaction with only one pulse is also shown. Taken from [15]

(b) Double expGauss and single expGauss are fit to hits in a single DOM from a ν_τ event.

Though the data looks like a gaussian distribution, a skewed normal gaussian and an Exponentially Modified Gaussian(expGauss) fit the data much better(fig 3.3). Here, the expGauss fit is chosen as it is more successful in fitting the data.

An expGauss is defined as in equation 3.3. It has an additional parameter, when compared to a regular gaussian, k . This parameter defines how exponential the tail of the gaussian is(fig 3.4a). By definition, the exponential tail, is always on the right side of the mean.

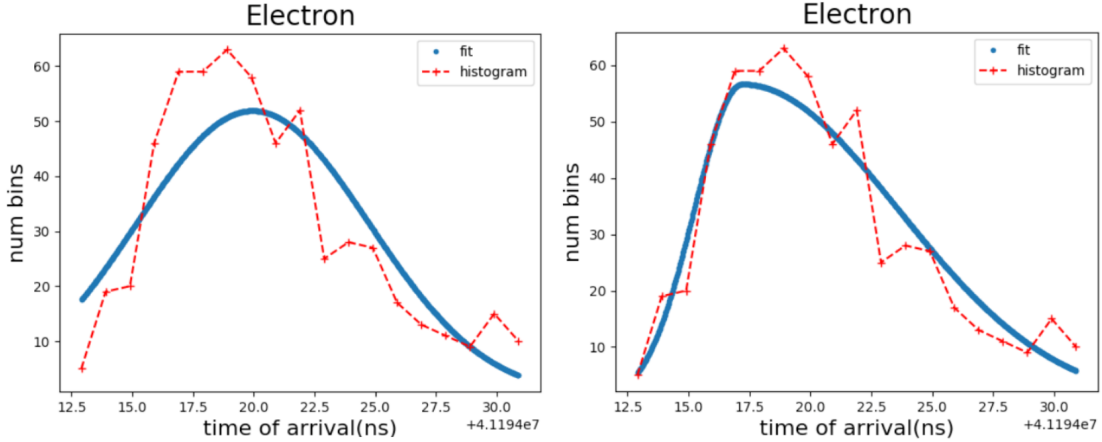
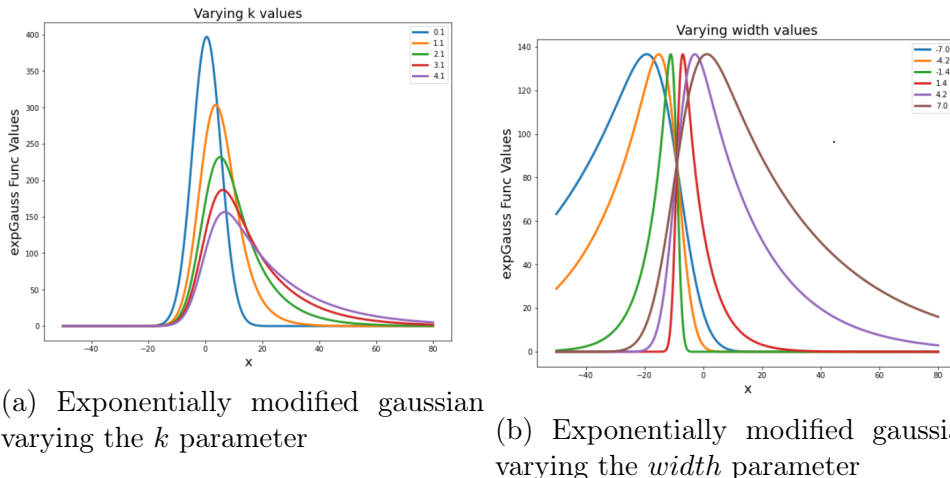


Figure 3.3: Gaussian vs Skewed Normal Gaussian

Giving the equation a negative width will result in the exponential tail on the left side of the mean (fig 3.4b).

$$f(x | \mu, \sigma, k, a) = a \frac{k}{2} \exp\left(\frac{k}{2} (2\mu + k\sigma^2 - 2x)\right) \operatorname{erfc}\left(\frac{\mu + k\sigma^2 - x}{\sqrt{2}\sigma}\right) \quad (3.3)$$



The double expGauss is simply the sum of two expGauss, therefore it has eight parameters. To see the separation of signal(double pulse) from background(single pulse) hits from each DOM in an event are fit with a double expGauss and a single expGauss.

3.3 The Algorithm

The algorithm uses the I3RecoPulses generated in the last step of the simulation chain. The algorithm loops each DOM per frame to retrieve hit information. A cut in the number of hits per DOM is imposed to remove DOMs that don't have enough statistics. The mean of the hits is calculated and then hits within 100 nanoseconds around the mean are selected (fig 3.5 [left]). These selected hits are then histogrammed with bin width = 3. The bin width depends on the PMT response given in section 2.3

The tails of the hit distributions affect the curve fit, to avoid this the tails are removed by setting entries ratio > 0.2 . Entries is ratio is defined in equation 3.4. This ensures that the tails are removed from the hit distribution. However, the discontinuity in the data is an issue(fig 3.5[center]). To avoid this the all the bins between the first bin and last bin in time that crossed the entries ratio threshold are selected(fig 3.5[right]). Two additional bins are included on either side of the selected bins.

$$\text{entries ratio} = \frac{\text{entries in each bin}}{\text{maximum bin entry}} \quad (3.4)$$

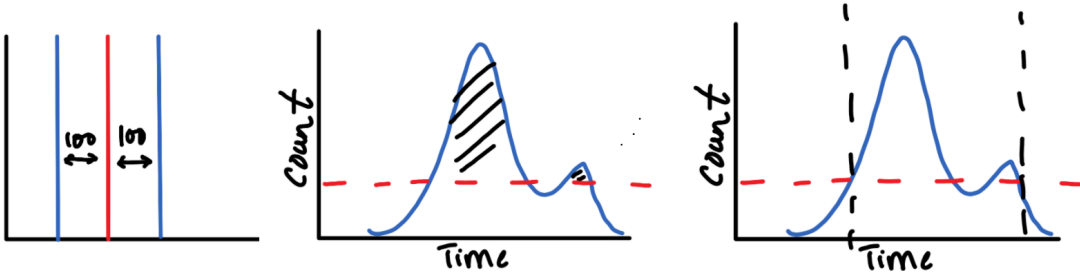


Figure 3.5: Left: Defining a time window. Center: Shaded regions are the selected bins Right: Selecting bins between the first bin in time and last bin in time that cross entries ratio threshold

As the double expGauss requires 8 parameters, the number of bins selected in the analysis should be greater than 8. The minimum bin requirement was set to 10. Therefore only DOMs with number of bins greater than 9 were only considered to fit an expGauss and double expGauss.

Once the DOMs are selected, the next step in the algorithm is to use minimize the negative log likelihood function, using IMINUIT minimizer, to get the best fit to the data. In cases where the errors are gaussian a chi-squared fit is sufficient to get a good fit. But the data used here is poisson distributed, therefore, a likelihood fit should be used. The binned likelihood is given by equation 3.5 [23]. The first term is model independent and can be ignored. Including this term causes the minimizer to return infinity. The minimizer returns the log likelihood(LLH) value and the parameters that define the expGauss and double expGauss.

$$-\ln L = \sum_i \ln(n_i!) + \mu_i - n_i \ln \mu_i \quad (3.5)$$

To check the credibility of the algorithm multiple tests were done. There is a significant impact of the bounds and initial values, given to the minimizer, on the fit(fig 3.6). The minimizer was very sensitive to the initial values given. To account for this, a grid search in width and k parameters was implemented.

3.4 Signal from Background

The parameters from double expGauss can be used to distinguish signal from background. For example, as seen in figure 3.2b the mean(position) of the two expGauss are sufficiently

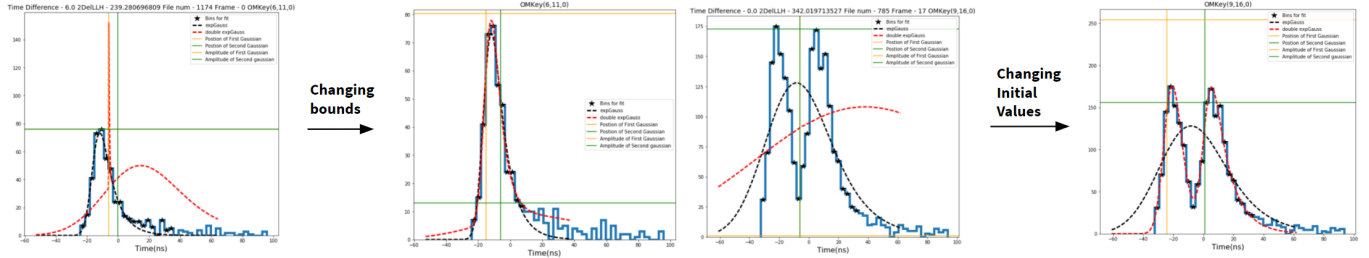


Figure 3.6: Changing the bounds and initial values improves the fit.

far apart to make out a double pulse signature. Therefore, calculating the difference between the two positions would show the separation between two expGauss. To start finding signal from the background the time difference(difference between mean), width difference, k difference and amplitude ratio are calculated. The last variable that will be used for the analysis here is the $2\Delta LLH$. Given by equation 3.6 this variable suggests how likely it is that the double expGauss is indeed the best fit to the data.

$$2\Delta LLH = 2 \times (LLH_{\text{double expGauss}} - LLH_{\text{expGauss}}) \quad (3.6)$$

The correlations between mean, width, k difference, amplitude ratio and $2\Delta LLH$ are plotted(fig 3.7 and fig 3.8). It turned out that the most separation between signal and background comes from the cut variable(log of $2\Delta LLH$). Cuts are introduced in this cut variable to extract the signal from the background.

For each cut value imposed, the DOMs with cut variable value greater than the cut values are selected. In fig 3.9[left] cut values in cut variable applied vs the corresponding number of DOMs selected shown. For higher cut values in the cut variable there is more probability that a selected DOM is from a ν_τ event(fig 3.9[right]).

To determine the number of ν_τ events in a year selected for every cut value, only one DOM per event is considered to avoid double counting and the weight of that event is applied. The weight of an event depends on the type of interaction. CC interactions can come from either astrophysical ν_τ or ν_e . But any flavored astrophysical neutrino can produce a NC interaction. Atmospheric muon neutrinos are also capable of producing NC interactions. Weights are calculated as per the type of neutrino interaction as shown in eq 3.7, eq 3.8 and eq 3.9 [24].

$$weight_{CC} = \frac{\phi_{astro} \times OneWeight \times LiveTime}{\frac{N}{4}} \quad (3.7)$$

$$weight_{NC,\nu_\mu} = \frac{(3\phi_{astro} + \phi_{atmo,\nu_\mu}) \times OneWeight \times LiveTime}{\frac{N}{2}} \quad (3.8)$$

$$weight_{NC,\bar{\nu}_\mu} = \frac{(3\phi_{astro} + \phi_{atmo,\bar{\nu}_\mu}) \times OneWeight \times LiveTime}{\frac{N}{2}} \quad (3.9)$$

where:

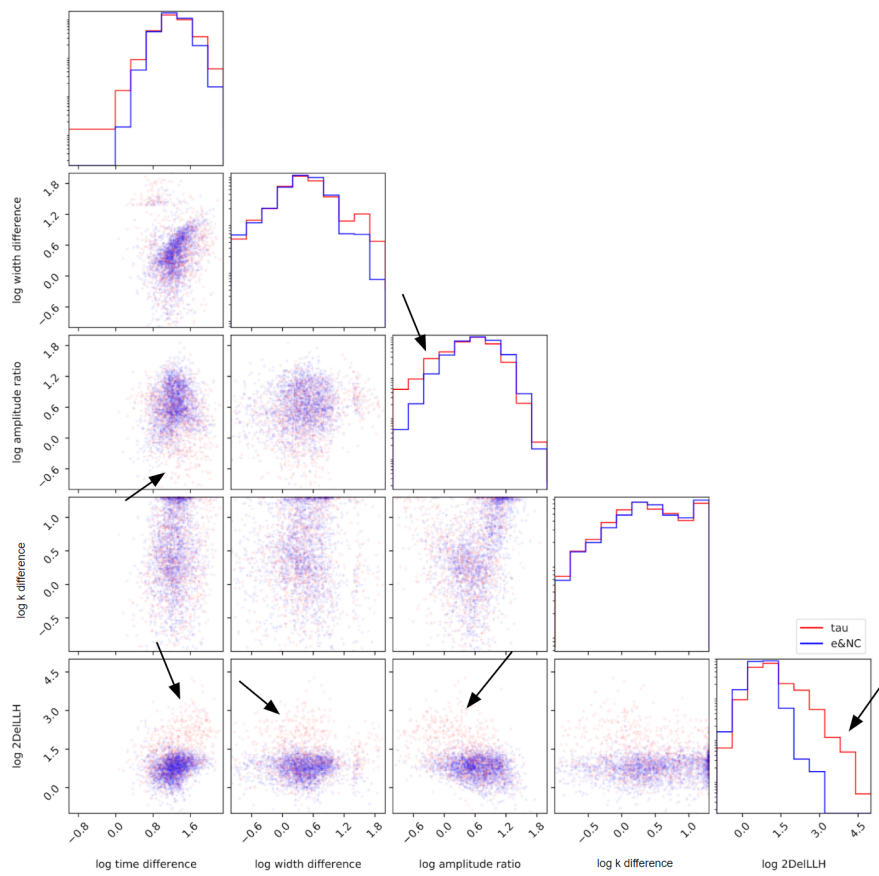


Figure 3.7: Correlation plot

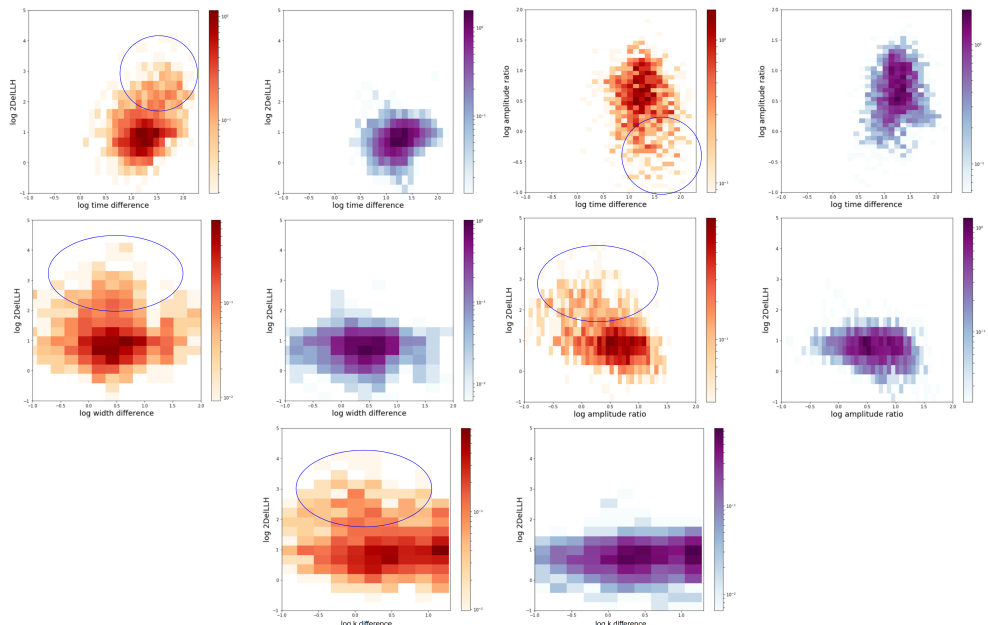


Figure 3.8: Correlation Plots as 2D Histograms. Orange: NuTau; Purple: Background

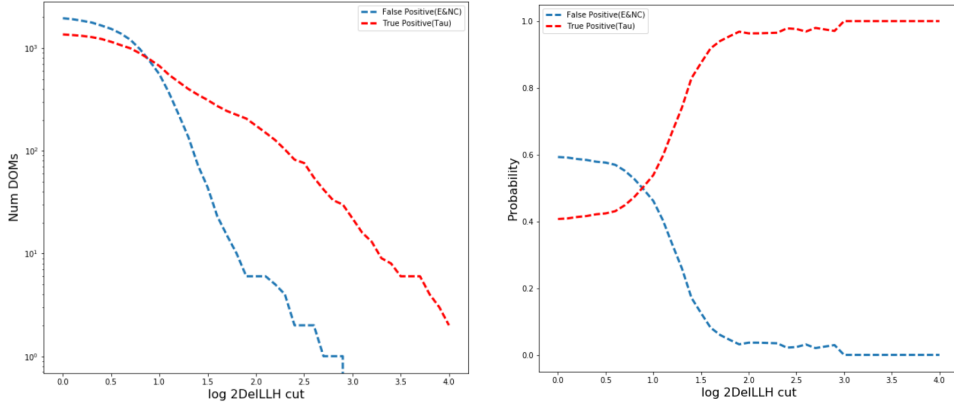


Figure 3.9: Left: Cut variable vs Number of DOMs. Right: Cut variable vs Probability. Red is the signal and blue is the background

$N/4$ = files contain 4 types of primary particles($\nu_\tau, \bar{\nu}_\tau, \nu_e, \bar{\nu}_e$)

$N/2$ = Considering ν and $\bar{\nu}$, flavour independent

Now with the weights included and one DOM per event the y axis in the plot(fig 3.10[left]) shows the number of events detected per year. At the intersection point of signal and background curves there is equal probability of the selected event being either ν_τ or background(fig 3.10[right]). The background events with large cut values come from events that see intense light(~50000 hits in a DOM) where it is impossible to identify a double pulse signature. In some cases the background events also show double pulse signals [Appendix D](#).

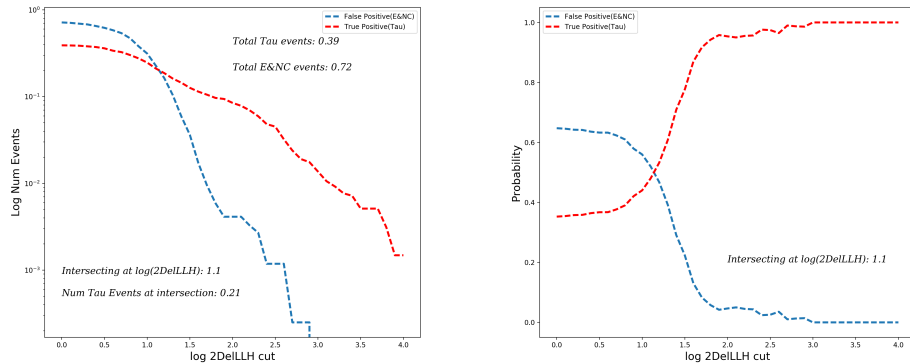


Figure 3.10: Left: Cut variable vs Number of Events. Right: Cut variable vs Probability. Red is the signal and blue is the background

In an ideal case at cut value zero, about 0.39 ν_τ CC events will be detected per year in P-ONE. But as seen in section 3.1 the expected ν_τ CC events per year is on the order of 1. This suggests that the algorithm needs to be revisited to improve the number of events per year.

3.5 Improving the Number of ν_τ events per year

The conditions imposed in selecting a DOM in section 3.3 were modified to increase the number of events in a year. A summary of changes made to the selection values is listed in figure 3.11.

Conditions Changed	Total NuE&NC Events	Total NuTau Events	Intersection Point	Tau Neutrino Events at Intersection Point
Number of hits in DOMs > 200	0.72	0.39	1.1	0.21
Number of hits in DOMs > 100	1.11	0.59	1.3	0.22
Number of hits in DOMs > 0	1.78	0.88	1.3	0.27
Number of bins ≥ 9	1.87	0.9	1.3	0.27
Entries Ratio > 0.1	2.1	0.97	1.5	0.28

Figure 3.11: Summary of changes made to the the DOM selection process

As the number of ν_τ events increase cut variable value at the intersection point(point at which there is equal probability of the event being a ν_τ or background) also increases. Though the increase in number of ν_τ events at the intersection point is not significant enough. Entries threshold of 0.1 was reverted to the original value of 0.2 as the increase in the intersection value is greater than the increase in the number of ν_τ events at the intersection point.

To verify, again, if the algorithm is working as expected, the correlation of cut variable with tau length is plotted(fig 3.12). As the tau length increases, the probability of seeing a double pulse signature also increases. So ideally large tau length would imply large cut variable value. But there are DOMs that populate the region where tau length is large and the cut variable is not large enough. The DOMs in this region come from events whose:

1. Interaction vertices lie outside the detector.
2. The tau generated decays into a muon, a muon does not produce a cascade, therefore there is no second expGauss. See [Appendix E](#) for exceptions
3. The photons from the two vertices reach the DOM at the same time making it impossible to distinguish between two expGauss. Or the DOMs are far away from either one of the vertex.

The energy distributions plotted of both the signal and background show that as the cut variable value increases the distribution shifts to the right(fig 3.13a and fig 3.13b).

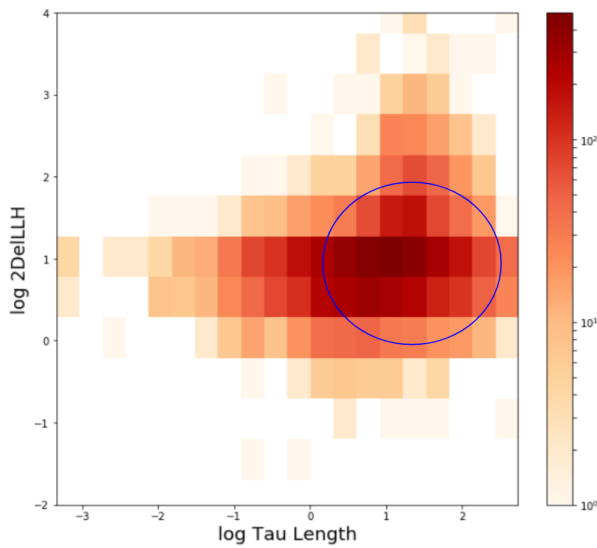
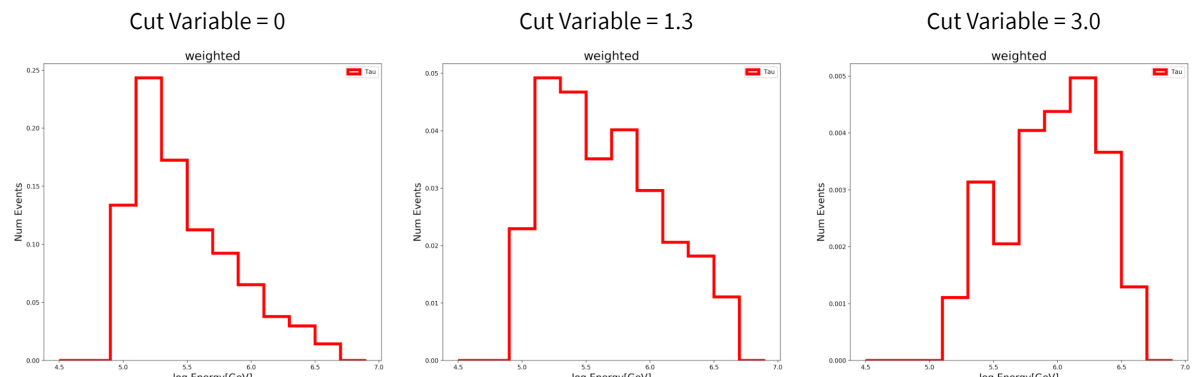
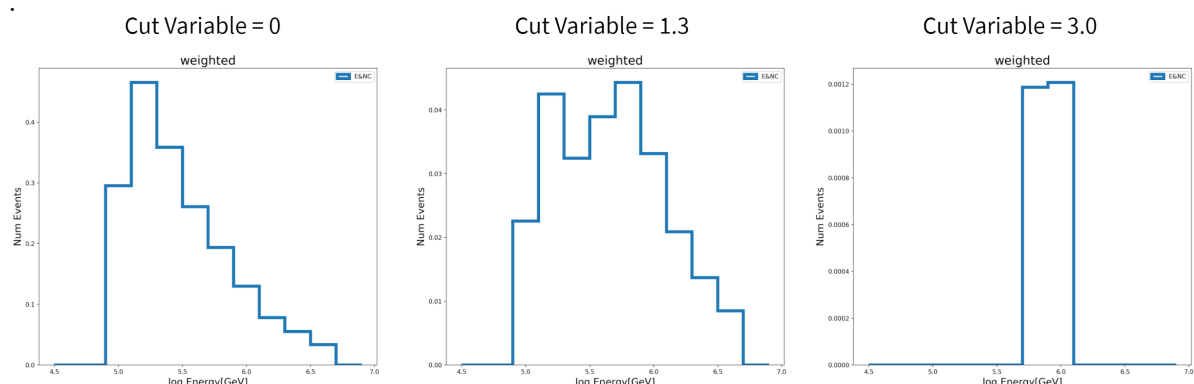


Figure 3.12: Tau length correlation plot



(a) Energy distributions of signal for a given cut variable



(b) Energy distributions of background for a given cut variable

Chapter 4

Conclusion and Next Steps

A complete simulation chain for P-ONE is produced using the IceCube software. A total of 40, 000 ν_τ and ν_e events are generated. CC interact of astrophysical ν_e , NC interactions of all flavoured astrophysical ν_e and NC interactions of atmospheric muon neutrinos are the major back ground from the study here. An IceCube mDOM is simulated and noise is injected from STRAW data.

However, there are certain aspects of the simulation that can be improved for example, in PROPOSAL the medium can be changed to water. The PMT response, which defines the bin width used for the analysis, can be improved. The bin width used for the current analysis is only 3ns, this can be made finer.

Approximately 1 ν_τ event per year is observed if the algorithm can identify all ν_τ double pulse signature from background. At greater than 1.3 cut variable value, only about 0.2 ν_τ events can distinguished from the background with a probability of greater than 0.5. This is already on par with IceCube. Within 5 years, using P-ONE phase 1 geometry, at least one ν_τ should be detected.

There is still a lot of scope in improving the algorithm. The DOMs with hits greater than or 50000 can be removed completely from the analysis. These DOMs have see very bright light making it impossible to see a double pulse signature in the hits distribution. There other parameters like the time difference, width difference, amplitude ratio and k difference are not used in the analysis. For certain number of hits in a DOM these parameters could perhaps be used to find signal from noise. Machine learning techniques can be implemented to enhance the existing separation between ν_τ and background.

Though for the ν_τ event the energy distribution with no cut(Cut variable = 0) peaks at 300TeV, there are is a possibility that simulating at lower energies can slightly increase the number of ν_τ detected in a year.

Bibliography

- [1] Yorikiyo Nagashima. *Elementary particle physics*. Vol. 1. Wiley Online Library, 2010 (page 1).
- [2] G Rajasekaran. “The Story of the Neutrino”. In: *arXiv preprint arXiv:1606.08715* (2016) (page 1).
- [3] Logan James Wille. *The Search for High Energy Tau Neutrinos using the IceCube Neutrino Observatory*. The University of Wisconsin-Madison, 2019 (pages 1, 4, 5).
- [4] M Agostini et al. “The Pacific Ocean Neutrino Experiment”. In: *arXiv preprint arXiv:2005.09493* (2020) (pages 1, 3).
- [5] *P-ONE: Why we need another neutrino telescope*. URL: <https://www.pacific-neutrino.org/p-one> (visited on 12/06/2020) (page 2).
- [6] *Where will P-ONE be located*. URL: <https://www.pacific-neutrino.org/p-one/where-p-one-will-be-located> (visited on 12/06/2020) (page 2).
- [7] *How P-ONE will be designed*. URL: <https://www.pacific-neutrino.org/p-one/how-p-one-will-be-designed> (visited on 12/06/2020) (page 3).
- [8] Francis Halzen and Spencer R Klein. “Invited review article: IceCube: an instrument for neutrino astronomy”. In: *Review of Scientific Instruments* 81.8 (2010), p. 081101 (pages 3, 5).
- [9] Hadiseh Alaeian. *An Introduction to Cherenkov Radiation*. URL: <http://large.stanford.edu/courses/2014/ph241/alaean2/> (visited on 12/06/2020) (page 3).
- [10] Gisela Anton. “Neutrino Telescopes”. In: *Probing Particle Physics With Neutrino Telescopes* (2019), p. 11 (pages 3, 4).
- [11] K Hamamatsu Photonics. “Photomultiplier tubes—basics and applications, 3rd edition”. In: *Hamamatsu Photonics* (2006) (page 3).
- [12] *About PMTs / Photomultiplier tubes (PMTs)*. URL: https://www.hamamatsu.com/jp/en/product/optical-sensors/pmt/about_pmts/index.html (visited on 12/06/2020) (page 4).
- [13] Andrea Palladino et al. “The importance of observing astrophysical tau neutrinos”. In: *Journal of Cosmology and Astroparticle Physics* 2018.08 (2018), p. 004 (pages 5, 6).
- [14] Maximilian Meier and Jan Soedingrekso. “Search for Astrophysical Tau Neutrinos with an Improved Double Pulse Method”. In: *arXiv preprint arXiv:1909.05127* (2019) (pages 5, 6).
- [15] Logan Wille and Donglian Xu. “Astrophysical Tau Neutrino Identification with IceCube Waveforms”. In: *arXiv preprint arXiv:1909.05162* (2019) (pages 5, 6, 20).
- [16] *OverView-What is IceTray?* URL: <https://docs.icecube.aq/simulation/V06-01-02/info/overview.html#what-is-icetray> (visited on 12/08/2020) (page 7).

- [17] Michael James Larson. “Simulation and identification of non-Poissonian noise triggers in the IceCube neutrino detector”. PhD thesis. University of Alabama Libraries, 2013 (page 7).
- [18] Christian Haack et al. “A measurement of the diffuse astrophysical muon neutrino flux using eight years of IceCube data.” In: *35th International Cosmic Ray Conference*. Vol. 301. SISSA Medialab. 2018, p. 1005 (pages 8, 19).
- [19] M Boehmer et al. “STRAW (STRings for Absorption length in Water): pathfinder for a neutrino telescope in the deep Pacific Ocean”. In: *Journal of Instrumentation* 14.02 (2019), P02013 (pages 10, 11).
- [20] MG Aartsen et al. “Measurement of South Pole ice transparency with the IceCube LED calibration system”. In: *Nuclear Instruments and Methods in Physics Research Section A: Accelerators, Spectrometers, Detectors and Associated Equipment* 711 (2013), pp. 73–89 (pages 12, 13).
- [21] JA Aguilar et al. “Transmission of light in deep sea water at the site of the ANTARES neutrino telescope”. In: *Astroparticle Physics* 23.1 (2005), pp. 131–155 (page 14).
- [22] Lew Classen and Alexander Kappes. “The multi-PMT optical module for the IceCube-Upgrade”. In: *EPJ Web of Conferences*. Vol. 207. EDP Sciences. 2019, p. 06004 (page 17).
- [23] Mark Thompson. *Fitting and Hypothesis Testing*. 2015. URL: https://indico.cern.ch/category/6015/attachments/192/631/Statistics_Fitting_II.pdf (page 22).
- [24] J.P. Yanez. Personal Communication. Nov. 2020 (page 23).

Appendix A

Testing PROPOSAL

The previous software release contained bugs in the code, with the tau decay products having the wrong direction. The new software update corrected this and using this updated PROPOSAL further tests were done.

A.1 Lepton Number

A ν_τ is always produced when a τ decays to conserve the lepton number. Although, this was not always the case, sometimes the τ decays into a ν_μ . This is corrected in another new release of the PROPOSAL(fig A.1).

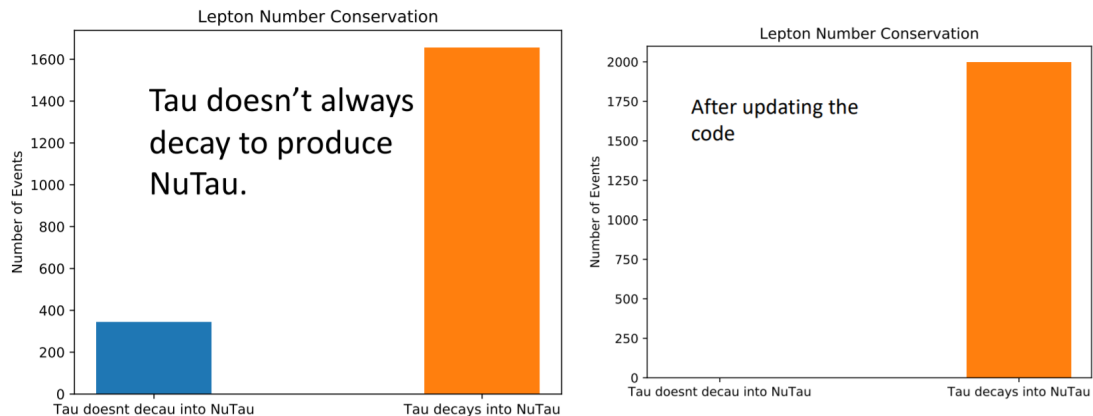


Figure A.1: Left: Lepton number is not conserved. Right: Lepton number is conserved after PROPOSAL is updated.

A.2 Book keeping in I3File

The I3MCTree stores all the stochastic energy losses of the τ . These stochastic energy losses are stored as daughters of the τ which makes it seem like a τ is decaying into a τ (fig A.2).

```

580 NuTau (481944m, 4.01059e+06m, -1.44077e+06m) (109.628deg, 83.1491deg) 0ns 1.18451e+06GeV 4.28869e+06m
582 TauMinus (91.1512m, -47.5417m, -145.404m) (109.63deg, 83.1493deg) 1.43055e+07ns 1.0275e+06GeV 10.3834m
585 TauMinus (91.1512m, -47.5417m, -145.404m) (109.63deg, 83.1493deg) 1.43055e+07ns 1.0275e+06GeV 5.93716m
586 Deltaf (90.4842m, -53.0939m, -143.41m) (109.63deg, 83.1493deg) 1.43055e+07ns 1.03448GeV 0m
587 TauMinus (90.4842m, -53.0939m, -143.41m) (109.63deg, 83.1493deg) 1.43055e+07ns 1.02727e+06GeV 0.00970105m
588 Deltaf (90.4842m, -53.0939m, -143.41m) (109.63deg, 83.1493deg) 1.43055e+07ns 1.03448GeV 0m
589 TauMinus (90.4831m, -53.103m, -143.406m) (109.63deg, 83.1493deg) 1.43055e+07ns 1.0275e+06GeV 4.43656m
590 MuMinus (89.9846m, -57.2518m, -141.916m) (109.63deg, 83.1491deg) 1.43055e+07ns 70511.9GeV nam
591 NuTau (89.9846m, -57.2518m, -141.916m) (109.63deg, 83.1494deg) 1.43055e+07ns 61314GeV 0m
592 NuMuBar (89.9846m, -57.2518m, -141.916m) (109.63deg, 83.1492deg) 1.43055e+07ns 335845GeV 0m

```

Taus are saved as daughters, but they are just undergoing stochastic energy loss

This is the tau that actually decays

Figure A.2: Book keeping in I3MCTree

A.3 Other Tests

The directions and energies of τ and τ decay products were also compared to check the working of PROPOSAL(fig A.3 and fig A.4). The difference on the x-axis in fig A.3 is defined as:

$$\text{Difference} = \tau \text{ Direction} - \tau \text{ Decay Product Direction} \quad (\text{A.1})$$

And the ratio on the x-axis in fig A.4 is defined as:

$$\text{Ratio} = \frac{\text{Sum of } \tau \text{ Decay Product Energies}}{\tau \text{ Energy}} \quad (\text{A.2})$$

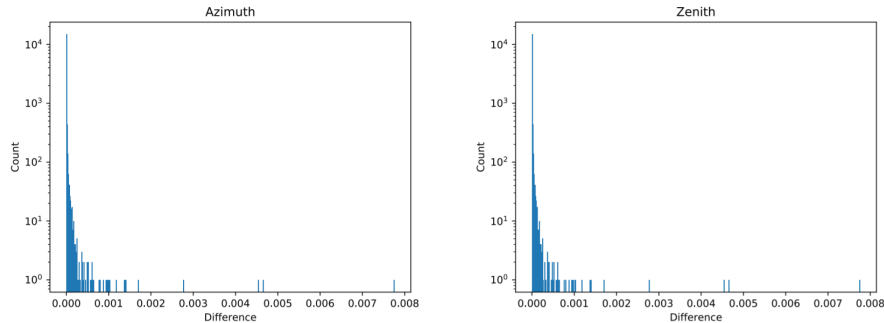


Figure A.3: Left: Difference in Azimuth. Right: Difference in Zenith

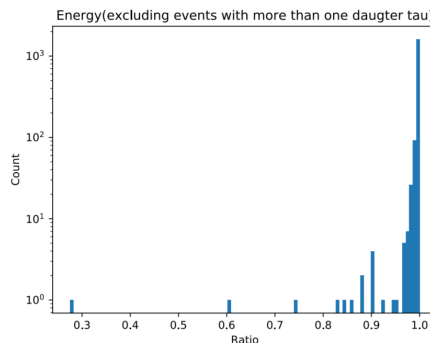


Figure A.4: Energy Ratio of τ and sum of τ decay products

Appendix B

Identifying the Center of Gravity of Hits

The idea of finding a DOM with double peak signature using Centre of Gravity(CoG) of hits was explored. The CoG is determined with respect to the center of the detector. CoG of hits is defined as:

$$\text{COM}_x = \frac{c_1 \cdot x_1 + c_2 \cdot x_2 + c_3 \cdot x_3 + \dots}{c_1 + c_2 + c_3 + \dots} \quad (\text{B.1})$$

where:

c_i = charge in i^{th} DOM.

x_i = Distance from center of detector to the i^{th} DOM.

DOMs with double peak were selected by imposing the time difference criteria that Δt is greater than 20 ns and less than 200 ns. Δt is $t_2 - t_1$ (fig B.1). DOMs selected this way contain double peaks but single peak structures are still observed.

There are a couple of defects with this method. The position of CoG depends on the event brightness(fig B.2b). The brighter the event the closer CoG is to the vertex of interaction(fig B.2a). And there is no definitive way of only selecting only double pulse signature DOMs for the analysis.

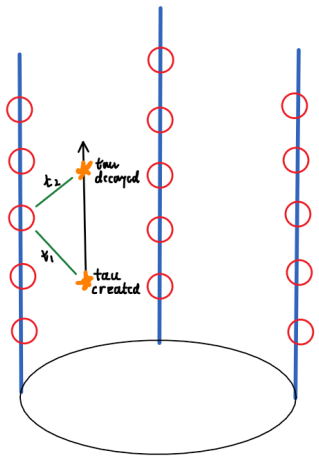
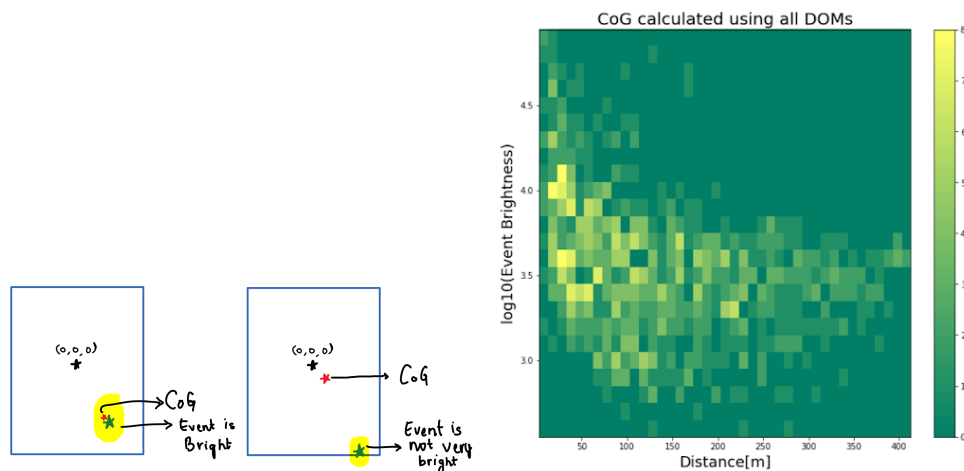


Figure B.1: t_1 and t_2 define the time taken by photons from vertices to reach a DOM.



(a) Location of CoG depends on the event brightness

(b) Plot shows the relation between the minimum CoG to DOM distance and the event brightness

Appendix C

Bifurcated gaussian

Before using an expGauss a skewed normal gaussian or bifurcated gaussian(biGauss) fit was used for separation of signal from background. BiGauss has an additional parameter, when compared to a regular gaussian, r . ' r ' defines how skewed a gaussian is.

Instead of a k difference, skewness difference is calculated. Using time difference, width difference, amplitude ratio, skewness difference parameters and 2 the signal is separated from background. The correlation plot is shown in figure C.1.

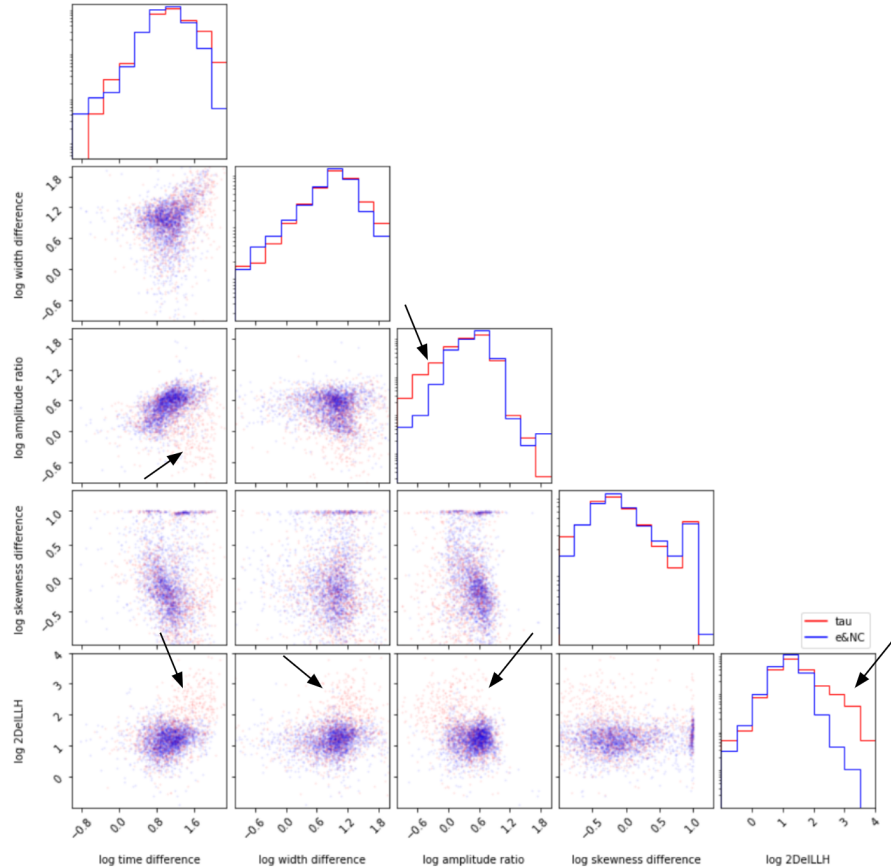


Figure C.1: Correlation plots for biGauss fits

There is not much difference in the separation of signal and background seen when compared to the expGauss. But an expGauss returns more successful fits.

Appendix D

Suspicious ν_e Event

A double peak signature is not only produced by ν_τ but also other physics events produce similar events (fig D.1). Although it is very rare that this happens. Only 1 event out of the 20,000 ν_e events simulated shows a prominent double peak signature.

A possibility here is that the high energy muon produced from the hadronic shower transfers its 4GeV energy to an electron. This energy is enough for an electron to start an electromagnetic shower. Since this electromagnetic shower started close to a DOM a prominent second peak has appeared in the DOM.

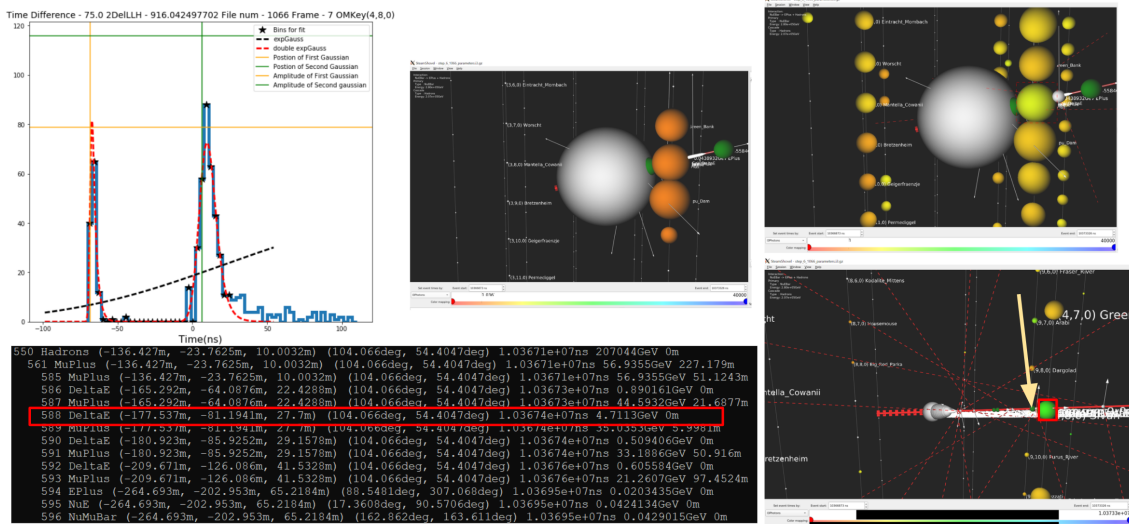


Figure D.1: DOM showing the double peak signature in ν_e event. Steamshovel used to view the event. Arrow indicates the region where the electromagnetic shower started. The red box beside the arrow indicates the DOM where the prominent double peak is observed.

Appendix E

Tau Decays into a muon

When a tau decays into a muon, there is no second cascade, therefore there is no second peak. There, however, are some exceptions to this as shown in figure E.1. But it is very uncommon that a double pulse signature is produced when a tau decays into a muon.

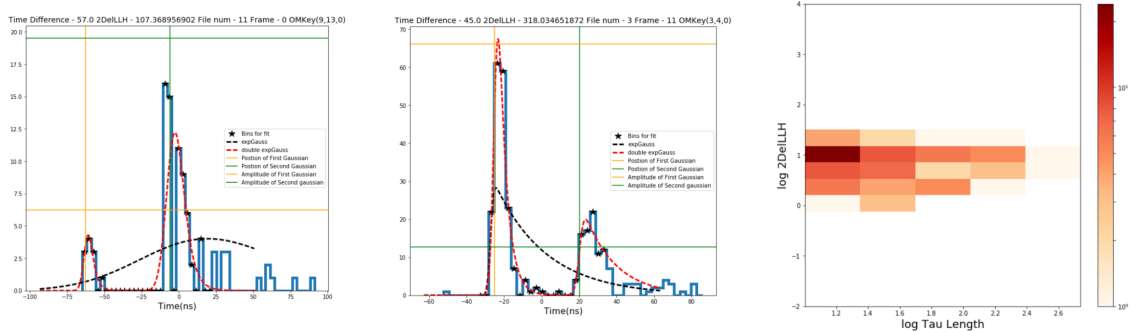


Figure E.1: First two plots show the exceptional cases where a double peak is observed when a tau decays into a muon. The last plot, 2D histogram, compares tau length against the cut variable of only events where a tau decays into a muon.

As seen in the 2D histogram in E.1, in cases where a tau decays into a muon the cut variable is below 1.5.

Appendix F

More on Next Steps

There is correlation between amplitude asymmetry and the cut variable. This was not inspected further.

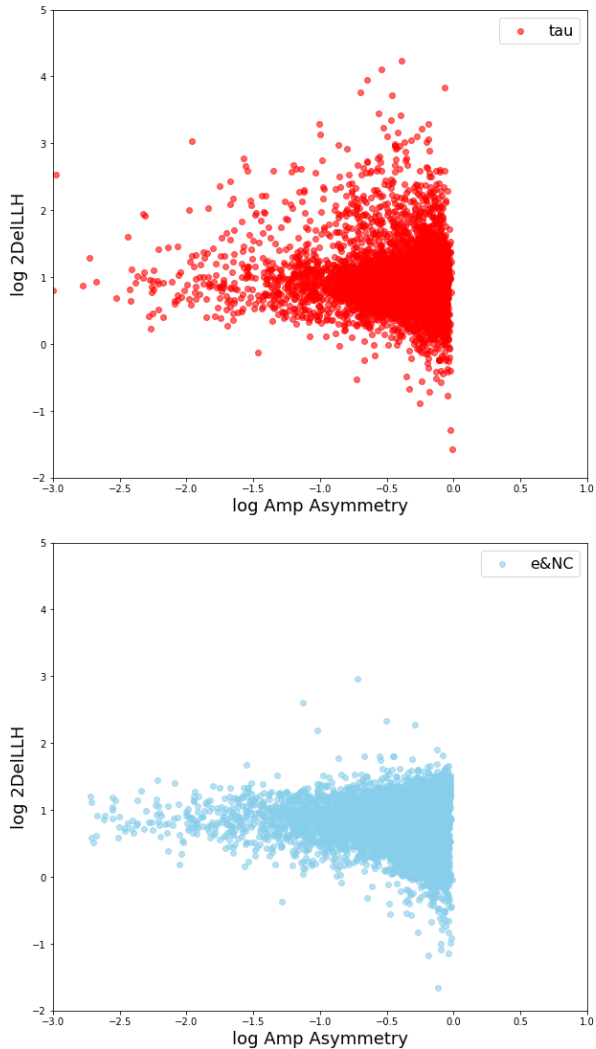


Figure F.1: The amplitude asymmetry plots for ν_τ and background events

The analysis method here used only a single DOM from each event. Using multiple DOMs

from a single event can improve the separation between ν_τ signal and background but also a couple ν_τ signals are rejected from the analysis.

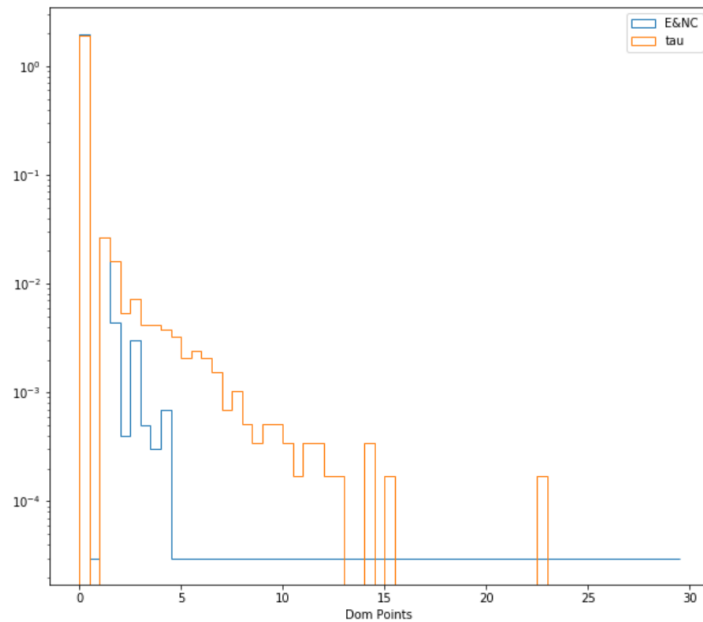


Figure F.2: DOM Points: Adding the cut variable values of DOMs in an event that have a cut variable value greater than a chosen threshold.

Appendix G

Documentation

G.1 Code

The scripts for the simulation and the analysis are on [gitHub](#).

G.2 Weekly, Analysis and Collaboration meet presentations

Presentations given during [local meetings](#), Bi-Weekly calls and [P-ONE collaboration meetings](#) are in folders in google drive.

G.3 Documenting Fits

Google slides on the changes done to the code to improve the analysis done in this study are [here](#).